

eRD14 - EIC PID consortium

- An integrated program for particle identification (PID) for a future Electron-Ion Collider (EIC) detector.

M. Alfred⁹⁾, L. Allison¹⁵⁾, M. Awadi⁹⁾, B. Azmoun³⁾, F. Barbosa¹³⁾, W. Brooks¹⁶⁾, T. Cao¹⁷⁾, M. Chiu³⁾, E. Cisbani^{11,12)}, M. Contalbrigo¹⁰⁾, A. Datta¹⁸⁾, A. Del Dotto¹¹⁾, M. Demarteau²⁾, J.M. Durham¹⁴⁾, R. Dzhygadlo⁸⁾, D. Fields¹⁸⁾, Y. Furletova¹³⁾, C. Gleason¹⁹⁾, M. Grosse-Perdekamp¹⁷⁾, J. Harris⁶⁾, X. He⁷⁾, H. van Hecke¹⁴⁾, T. Horn⁴⁾, J. Huang³⁾, C. Hyde¹⁵⁾, Y. Ilieva¹⁹⁾, G. Kalicy⁴⁾, M. Kimball¹⁾, E. Kistenev³⁾, Y. Kulinich¹⁷⁾, M. Liu¹⁴⁾, R. Majka⁶⁾, J. McKisson¹³⁾, R. Mendez¹⁴⁾, P. Nadel-Turonski¹³⁾, K. Park¹³⁾, K. Peters⁸⁾, T. Rao³⁾, R. Pisani³⁾, Yi Qiang¹³⁾, S. Rescia³⁾, P. Rossi¹³⁾, M. Sarsour⁷⁾, C. Schwarz⁸⁾, J. Schwiening⁸⁾, C.L. da Silva¹⁴⁾, N. Smirnov²⁰⁾, H. Stien¹⁾, J. Stevens⁵⁾, A. Sukhanov³⁾, S. Syed⁷⁾, A. Tate¹⁾, J. Toh¹⁷⁾, C. Towell¹⁾, R. Towell¹⁾, T. Tsang³⁾, R. Wagner²⁾, J. Wang²⁾, C. Woody³⁾, C.-P. Wong⁷⁾, W. Xi¹³⁾, J. Xie²⁾, Z.W. Zhao⁶⁾, B. Zihlmann¹³⁾, C. Zorn¹³⁾.

¹⁾ Abilene Christian University, Abilene, TX 79601

²⁾ Argonne National Lab, Argonne, IL 60439

³⁾ Brookhaven National Lab, Upton, NY 11973

⁴⁾ Catholic University of America, Washington, DC 20064

⁵⁾ College of William & Mary, Williamsburg, VA 2318

⁶⁾ Duke University, Durham, NC 27708

⁷⁾ Georgia State University, Atlanta, GA 30303

⁸⁾ GSI Helmholtzzentrum für Schwerionenforschung GmbH, 64291 Darmstadt, Germany

⁹⁾ Howard University, Washington, DC 20059

¹⁰⁾ INFN, Sezione di Ferrara, 44100 Ferrara, Italy

¹¹⁾ INFN, Sezione di Roma, 00185 Rome, Italy

¹²⁾ Istituto Superiore di Sanità, 00161 Rome, Italy

¹³⁾ Jefferson Lab, Newport News, VA 23606

¹⁴⁾ Los Alamos National Lab, Los Alamos, NM 87545

¹⁵⁾ Old Dominion University, Norfolk, VA 23529

¹⁶⁾ Universidad Técnica Federico Santa María, Valparaíso, Chile

¹⁷⁾ University of Illinois, Urbana-Champaign, IL 61801

¹⁸⁾ University of New Mexico, Albuquerque, NM 87131

¹⁹⁾ University of South Carolina, Columbia, SC 29208

²⁰⁾ Yale University, New Haven, CT 06520

Contacts: P. Nadel-Turonski <turonski@jlab.org>, Y. Ilieva <jordanka@physics.sc.edu>

Table of Contents

1. Introduction

2. Hadron Identification

2.1 PID requirements and implementation options

2.1.2 Hadron ID requirements

2.1.3 Integrated PID solution for the EIC (concept) detector(s)

2.2 Dual-radiator RICH

2.2.1 Dual-radiator RICH: Simulation and Performance

2.2.2 FY16 Progress and Achievements

2.2.3 Proposed Dual-radiator RICH R&D Activities

2.2.4 Dual-radiator RICH R&D Deliverables

2.3 Modular Aerogel RICH (mRICH)

2.3.1 FY16 Progress and Achievements

2.3.2 Proposed mRICH R&D Activities

2.3.3 mRICH R&D Deliverables

2.4 DIRC

2.4.1 High-performance DIRC: Simulations and Performance

2.4.2 FY16 Progress and Achievements

2.4.2.1 Hardware: Development and Validation of the 3-layer Spherical Lens

2.4.2.2 Software: Simulation

2.4.3 Proposed DIRC R&D Activities

2.4.4 DIRC R&D Deliverables

2.5 High-resolution Time-of-Flight (TOF)

3. Lepton (electron) Identification

4. Photosensors & Electronics

4.1 Sensors in High-B fields

4.2 LAPPDs

4.3 GEM photocathodes

4.4 Readout Sensors and Electronics for Detector Prototypes

5. Budget

Appendices

Appendix A: List of Publications and Presentations

Abstract

The EIC PID consortium (eRD14) has been formed to develop an integrated program for particle identification (PID) for a future Electron-Ion Collider (EIC) detector, for which excellent particle identification is an essential requirement. For instance, identification of the hadrons in the final state is needed for understanding how different quark flavors contribute to the properties of hadrons, and reliable identification of the scattered electron is important for covering kinematics where pion backgrounds are large. The PID systems also have the greatest overall impact on the layout of the central detector, and put important constraints on the magnetic field. It is thus essential to conduct the relevant R&D at an early stage of the development of a complete EIC detector. In addition to providing solutions addressing the broader EIC requirements, the PID consortium has worked closely with BNL and JLab to ensure that the specific R&D projects are compatible with the detector concepts that are being pursued there.

1. Introduction

The ability to identify hadrons in the final state is a key requirement for the physics program of the EIC. Being able to tag the flavor of the struck quark in semi-inclusive DIS can, for instance, tell us something about the transverse momentum distributions (and potentially orbital angular momentum) of the strange sea, while open charm (with subsequent decays into kaons) is important for probing the distribution of gluons in protons and nuclei. While the distribution of produced particles depends on the specific process, broadly speaking the kinematics for meson production follow the energies of the colliding beams. If the scattering produces a meson traveling in the direction of the proton (ion) beam, this meson can have a momentum which is a significant fraction of that of the original proton (high x or Q^2). If the meson is produced in the opposite (electron) direction, it cannot acquire more momentum than that carried by the electron beam. In the central region, it is possible to produce a range of momenta in-between, but the dominant effect is the strong dependence of the cross section on the transverse momentum component (p_T), which in this angular (rapidity) range is close to the total meson momentum. However, while there are fewer mesons with high momenta in the barrel than in the electron-side endcap, the physics relevance of the high- p_T events is not diminished, and hence the momentum range needed for hadron identification in the central barrel is only somewhat lower.

To address the different requirement associated with the three different parts of the detector, the consortium is pursuing R&D on (and requesting funding for) three different technologies for imaging Cherenkov detectors: a dual-radiator (gas/aerogel) RICH for the hadron endcap, a high-performance DIRC for the barrel region, a modular aerogel RICH (mRICH) for the electron endcap (which could also be used in the hadron endcap in conjunction with a single-radiator gas RICH such as the one developed by eRD6). A 4π time-of-flight (TOF) coverage is also needed for PID in the momentum range below the Cherenkov threshold and for bunch identification (which is important for ring-ring colliders with a high repetition rate), for which the consortium has performed R&D on mRPC and MCP-PMT based TOF systems.

The Cherenkov systems also have a significant potential for e/π identification (for momenta up to about 20 GeV/ c for the dual-radiator RICH and up to 1.7 GeV/ c for the DIRC), providing an important capability supplementing the electromagnetic calorimeters and other possible e/π ID systems. In an electron-ion collider, detection and identification of the scattered electron is a crucial capability. Here, a

challenge is posed by the charged pion background, which rises rapidly at lower momenta. Thus, to access kinematics where the scattered electron has low momentum one needs a good pion suppression. But electron identification is also important for measuring particles decaying into higher-momentum leptons. Examples include exclusive J/ψ production, used for transverse imaging of gluons in protons and nuclei, and spectroscopy of exotic (XYZ) states, for which the capabilities of the dual-radiator RICH are well suited. However, while we are not requesting funding for this in FY17, it would be natural to eventually (in FY18?) extend the R&D to systems specifically aimed at e/π identification (such as an endcap HBD). Since e/π systems cross technology boundaries, it would be important to coordinate such R&D with other consortia (*e.g.*, eRD6).

The PID consortium is also carrying out R&D on photosensors for these Cherenkov detectors. The challenges addressed by the PID consortium are: Operations inside the magnetic field of the central detector; and Cost reduction. The former is carried out using the high-B test facility at JLab, while the latter focuses on adaptation and optimization of LAPPDTM MCP-PMT's to EIC requirements (pixelized readout, UV photocathodes, high-B capabilities), as well as characterization of early-production sensors. In FY17 we are also proposing to start an effort within the consortium focused on standardizing photosensors and developing common readout electronics for different prototyping efforts. Being able to use the same sensors and electronics for multiple prototypes can lead to very significant cost savings during the R&D phase. In the longer term (FY18 and beyond), we are also considering developing a strategy for sensors and readout for all the PID systems, exploring how to best utilize the synergies among them.

2. Hadron identification

2.1 PID requirements and implementation options

2.1.1 Hadron ID requirements

The physics program of the EIC, as described in the White Paper, the 2010 INT report, the 2015 NSAC Long Range Plan, and elsewhere, is very broad and multifaceted - and so are the corresponding detector requirements. The most basic particle distribution is that from inclusive Deep Inelastic Scattering (DIS), which essentially sums over all combinations of final-state hadrons for a given kinematics (x , Q^2) of the scattered electron. As one looks at specific subsets of the data, the particle distributions can be quite different. As an example, analysis of events at the exclusive limit leads to transverse spatial imaging of the quarks and gluons in the target nucleon or ion beam (flavor sensitivity is crucial, to unravel the chiral symmetry breaking structure of the sea). Here, the struck quark hadronizes into a pion or kaon, taking essentially all of the momentum transferred from the scattered electron. In this subprocess, the kaon momenta are much higher than the average for kaon production in DIS. Similarly the intermediate case of semi-inclusive DIS allows the creation of transverse images in momentum space. Here it is also important to cover a wide range in meson momentum fraction (*vis a vis* the 'jet'), with PID for flavor separation. Failing to do so will restrict the kinematical reach of the the EIC regardless of the beam energies provided by the accelerator.

Another important case to consider is when the kaons are not produced in the primary process, but are decay products of heavier mesons. For instance, the kaons from the decay of the ϕ -meson, which is important for studies of gluon saturation, have higher momenta than kaons from the decay of D-mesons (open charm), which also provide information on gluon distributions.

To compile a catalogue of processes and kinematics illustrating the impact of various kaon identification options on the full EIC physics program goes beyond the scope of this R&D proposal. A lot of information can be found in the EIC White Paper, to which we refer. However, we note that for the purpose of understanding the general hadron ID requirements at EIC, this level of detail is not necessary. As long as one keeps in mind that a lot of the information lies in the tails of the distributions, where the number of particles is small, the meson distributions from inclusive DIS provide a good guidance. Figure 1.1.1 shows these distributions for pions and kaons in a common BNL/JLab kinematic (10 GeV electrons on 100 GeV protons), in a broad but typical bin of Q^2 .

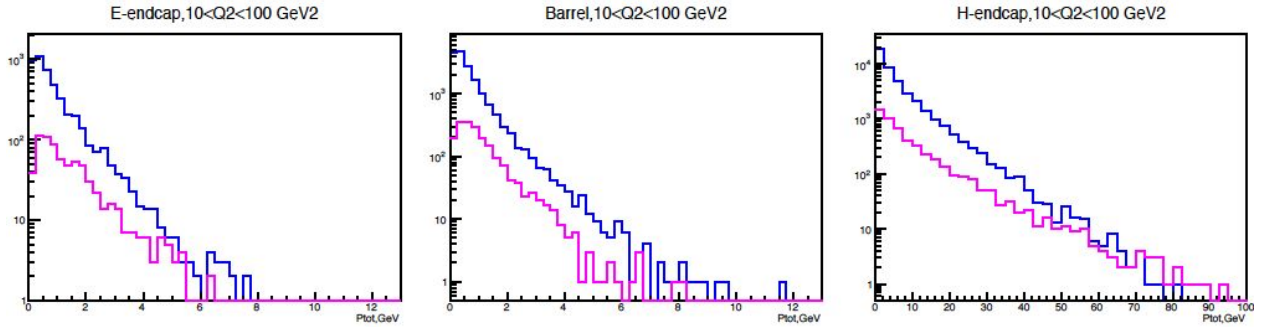


Figure 1.1.1 Momentum distributions for pions (blue) and kaons (magenta) from pythia for DIS events corresponding to collisions between 10 GeV electrons and 100 GeV protons, a common BNL/JLab kinematic, shown for a bin of $10 < Q^2 < 100 \text{ GeV}^2$ (without imposing cuts related to any specific physics channel or analysis).

As discussed in the introduction, with higher beam energies, the meson energies in the endcaps become correspondingly higher, while the distribution in the central barrel (which also reflects the p_T distribution), is less affected. Figure 1.1.1 clearly shows the need for PID over a very wide range (up to about 50 GeV) in the hadron endcap, and a moderate range up to 5-7 GeV in the central barrel. In the electron endcap, which also sees hadrons with higher momenta produced at lower values of Q^2 , the desired range would reach somewhat higher than the Q^2 -bin in Figure 1.1.1 suggests, approaching the electron beam energy. Thus, an upper limit of about 10 GeV is a relatively site-independent requirement. In addition, we note that the π/K ratios are not excessive - and tend to become smaller for higher momenta, which makes identification easier. Thus, when discussing the momentum reach, the relevant level of separation is 3-4 σ .

2.1.2 Integrated PID solution for the EIC (concept) detector(s)

The three model detectors developed at BNL and JLab have slightly different layouts of the hadron ID systems, some of which have been worked out in detail, and some of which are still placeholders. The approach chosen by the PID consortium is to develop an integrated solution that would be suited for the EIC physics requirements, while maintaining a compatibility with both the accelerator energies proposed at BNL and JLab, and the concept detectors developed there (shown in Figures 2.1.1-2.1.3).

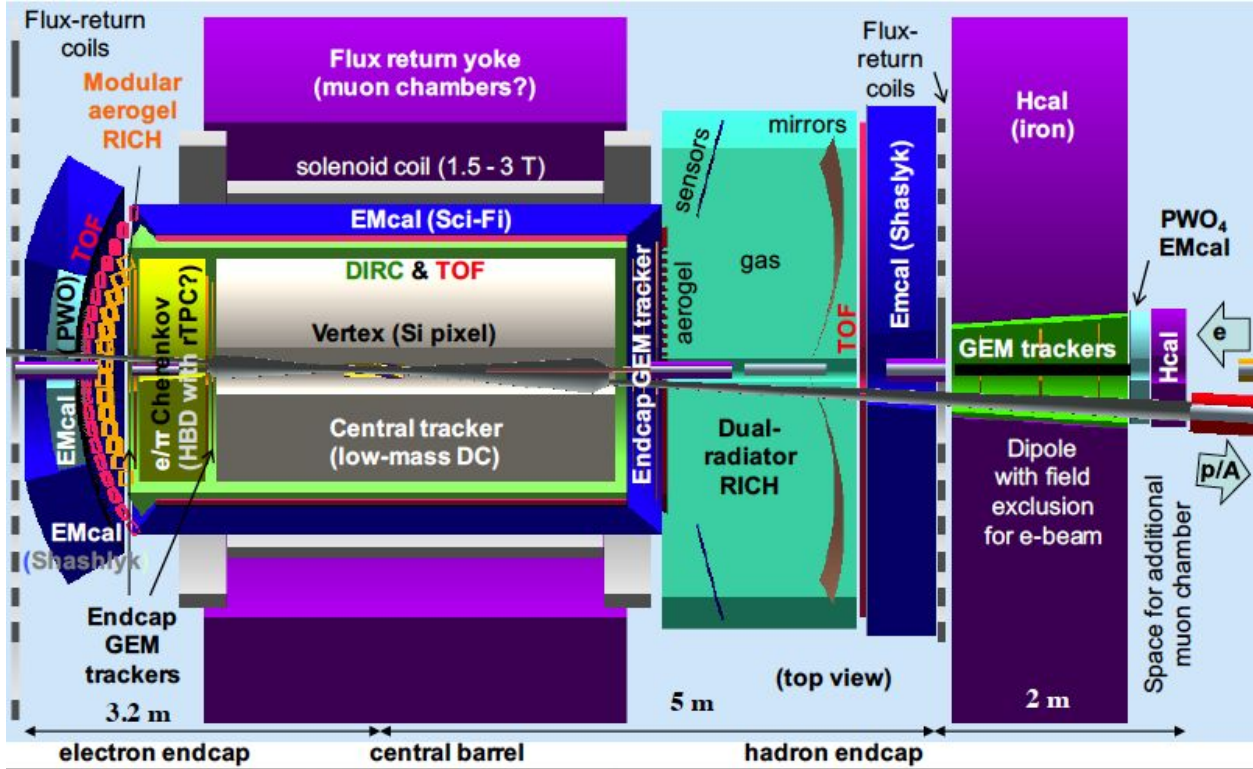


Figure 2.1.1 The JLab central detector concept uses the DIRC, dual-radiator and modular aerogel RICH detectors from the eRD14 R&D, and has 4π TOF coverage. It also includes an e/π Cherenkov in the electron endcap.

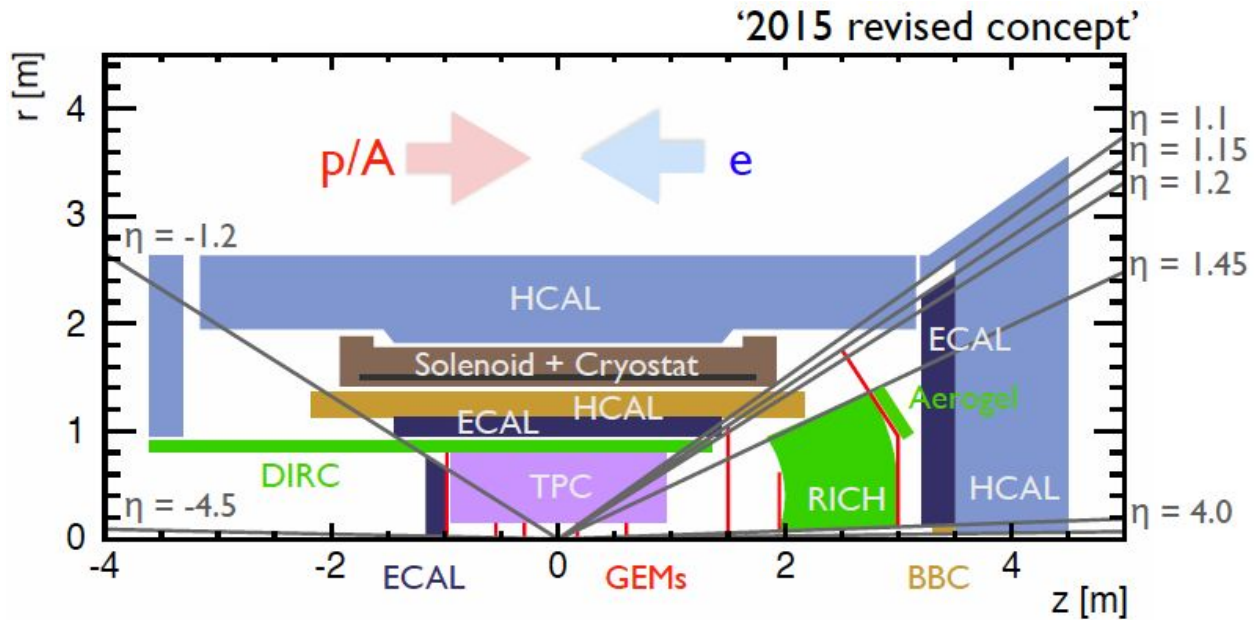


Figure 2.1.2 The 2015 BNL ePHENIX detector concept, based on the BaBar solenoid, proposes a DIRC at mid-rapidity and a modular aerogel RICH from eRD14, the latter together with a single-radiator gas RICH developed within eRD6. However, the DIRC could be replaced with TOF. The hadron endcap is compatible with a dual-radiator RICH or a combination of TOF+RICH, and the electron endcap is compatible with a modular aerogel RICH and/or an e/π Cherenkov.

-4< η <4: Tracking & e/m Calorimetry (hermetic coverage)

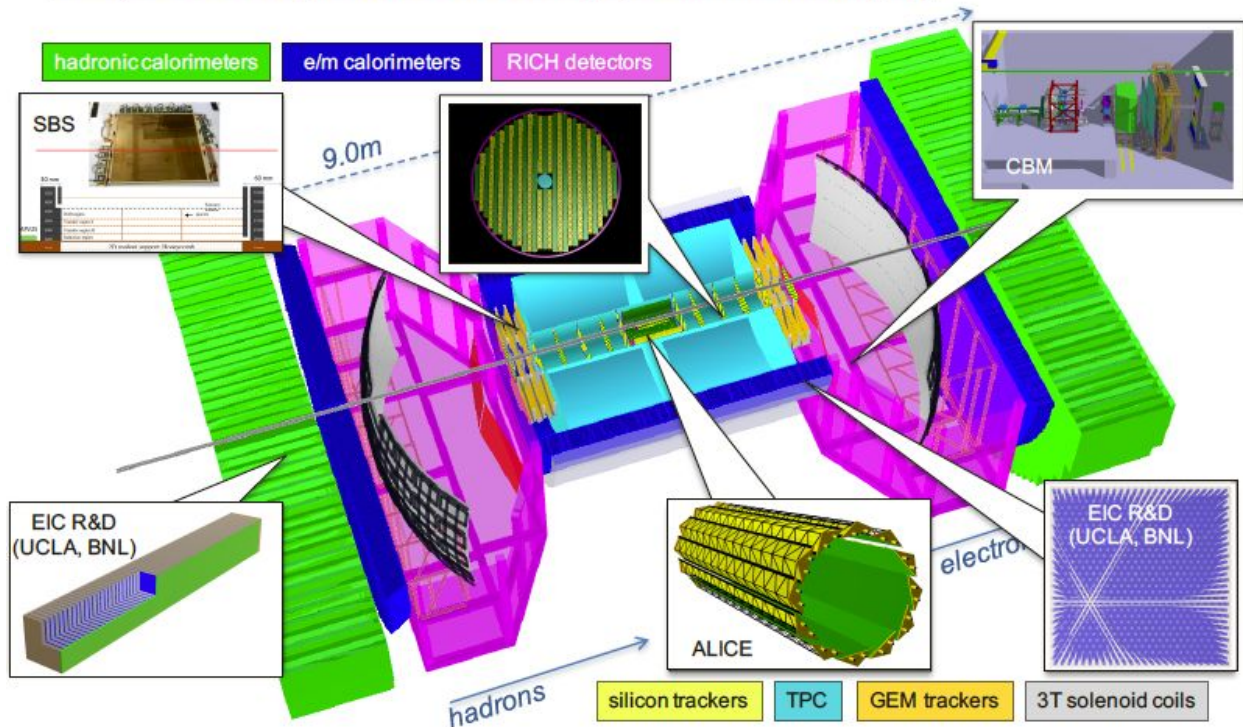


Figure 2.1.3 The BNL BeAST central detector concept in its nominal configuration only uses two hadron ID detectors - a RICH detector on each side based on the one from the CBM experiment at GSI (the CBM RICH model came with the simulation package). However, it would be relatively straightforward to replace the CBM RICH with a dual-radiator RICH concept developed for the EIC by eRD14. And on the side of the electron endcap, the modular aerogel RICH may provide a more compact and attractive solution, well matched to the EIC requirements. Given the small-diameter solenoid used in the BeAST detector, the radially-compact DIRC would be an ideal hadron ID solution for the central barrel.

In addition to the physics requirements and the desire to reach a reasonable level of compatibility with the three model detectors, two additional criteria were also considered in the choice of subsystems: cost and space requirements.

Central Barrel

The decision to pursue the DIRC as the baseline solution was based on several considerations. First, using recent estimates for the cost per unit area covered, polished fused silica is considerably cheaper than even the most optimistic estimates for low-cost photosensors (such as LAPPDs). The DIRC is also by far the most radially compact solution, and has already been incorporated into the design of two of the model detectors (JLab and ePHENIX), but would also be straightforward to incorporate into the third one (BeAST). The only initial concern was that the state-of-the-art momentum coverage (BaBar) of 4 GeV/ c would be marginal in terms of PID requirements. However, the eRD4 project demonstrated that a high-performance DIRC was possible with a momentum reach very well matched to the PID requirements for an EIC. Furthermore, eRD14 (EIC PID) has shown in its first year that with time-based reconstruction

algorithms, it may even be possible to increase the momentum reach beyond the 50% beyond state-of-art that was the original goal, or to reduce cost by moving to wider bars (plates). Other solutions for PID in the barrel that have been considered include either a high-performance TOF or an aerogel RICH.

(Outgoing) electron-side endcap

The EIC is designed for supporting a wide range of electron energies (currently assumed to be 3-12 GeV in the first stage of the JLab design and up to 20 GeV at BNL). The maximum hadron energy (as well as rate) in the hadron endcap increases with electron beam energy, and a dedicated hadron ID system for the electron endcap becomes progressively more important. However, a target of value for the coverage of around 10 GeV would satisfy both the BNL and JLab requirements. In terms of the model detectors, this is the area where they differ most: ePHENIX currently has no preference but will select from the technologies developed in eRD14, the BeAST has one similar to the one on the hadron side, where momenta are much higher, while the JLab detector uses the (modular) aerogel RICH developed by the PID consortium. However, these different assumptions do not reflect fundamentally different ideas or physics priorities - and there seems to be a consensus in the community that coverage up to about 10 GeV/c, which can be reached using an aerogel RICH, would be a good solution for any EIC detector. Starting with this assumption, there are two ways to proceed - either through a mirror-based design (conceptually similar to what, for instance, is being pursued for CLAS12), or the modular, lens-based aerogel RICH. The key advantage of the latter is compactness, which simplifies integration and reduces the cost of the endcap calorimeters. The latter may affect cost more than the reduction in sensor area possibly achievable in a mirror-based configuration. The consortium also aims to reduce costs through the proposed sensor R&D. Since R&D on mirror-based aerogel designs is performed elsewhere (e.g. CLAS12), and the novel modular concept seems to be a very good match for any EIC detector, this technology was selected as the main focus of the PID consortium R&D. Another advantage of pursuing this avenue is also that the same detector type could be used in a supplementary role to provide partial coverage on the hadron endcap in conjunction with a single-radiator gas RICH.

(Outgoing) hadron-side endcap

Due to the large hadron momenta, the PID requirements on the hadron endcap are in many way the most demanding. The difference in maximum beam proton energies between the two accelerators considered (250 GeV for BNL and 100 GeV for the first stage at JLab), which drives the required PID range, is also significant. However, even for lower beam energies (100 GeV), the hadron momenta are so large that there is a clear benefit of extending the momentum coverage for hadron ID to 50 GeV/c (and electron ID up to 15-20 GeV/c), and even a system built to a minimum requirement would need to incorporate a mirror-based, focusing gas RICH as part of the PID solution. From a technological point of view, the R&D path that needs to be pursued for the hadron ID is thus relatively site-independent. Rather, the key challenge and design choice is how to best cover the full momentum range. A path pursued earlier by the eRD6 (for ePHENIX) was to develop a single-radiator CF_4 gas RICH with inward-reflecting mirrors and a windowless, near-beam CsI GEM-based readout (UV only). To cover the lower momenta, ePHENIX could use an outer ring of the modular aerogel RICH detectors discussed above, covering part of the hadron endcap, and/or have full coverage of high-precision TOF. While this is a valid concept, in FY16 the PID consortium started developing a dual-radiator RICH, which provides full momentum coverage

over all forward angles and is the baseline choice for the JLab detector and the BeAST, and could also be an option for ePHENIX.

Aerogel($n = 1.02$) | $e_{th}(GeV/c) = 0.0025$ | $\pi_{th}(GeV/c) = 0.67$ | $K_{th}(GeV/c) = 2.46$ | $p_{th}(GeV/c) = 4.89$
C₂F₆($n = 1.00082$) | $e_{th}(GeV/c) = 0.0123$ | $\pi_{th}(GeV/c) = 3.48$ | $K_{th}(GeV/c) = 12.3$ | $p_{th}(GeV/c) = 23.4$

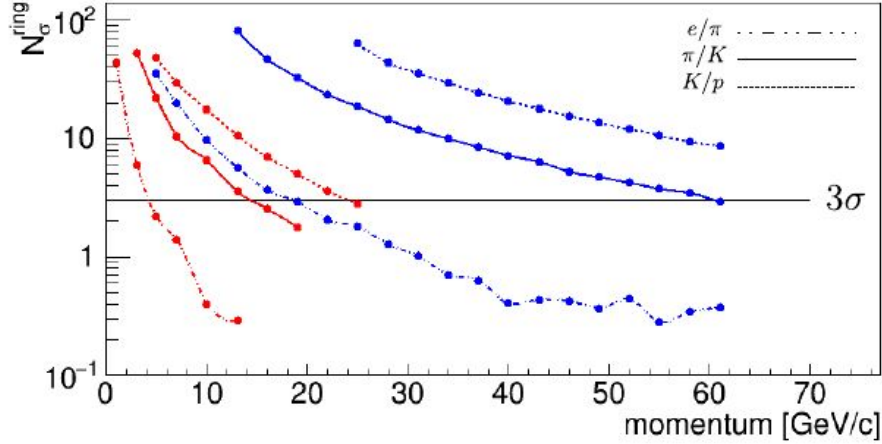


Figure 2.1.4 C₂F₆ gas/aerogel dual-radiator RICH performance for a particle at 15 degrees. There is good overlap in PID for all three species pairs with the Aerogel (red) and gas (blue).

Time-of-Flight (TOF)

The Cherenkov detectors described above not only provide PID, but also have good timing resolution. However, they do not provide a signal for particles below threshold (*i.e.*, slower than light in the radiator medium). Thus, for PID below the range of the aerogel RICH or DIRC detectors, a different method is needed. This could be accomplished through dE/dx in the tracker or by using a dedicated TOF system. In addition to PID, the latter also offers the possibility to uniquely associate particles with a certain bunch (particularly important for high-frequency colliders) and to correlate particles in the central detector with near-beam hadron and electron detectors located at some distance. While a baseline capability could be provided by scintillator-based TOF detectors (CLAS12, designed to operate at $10^{35} \text{ cm}^{-2}\text{s}^{-1}$ luminosity with a 2 ns bunch spacing, has simple TOF counters with 80 ps resolution), mRPC and MCP-PMT based TOF systems can be highly-segmented, and have the potential to provide very good timing resolution. They are also made of inexpensive materials, and R&D into construction methods could significantly lower the cost. Thus, we feel that at this stage of the EIC R&D program, it would be valuable to explore the full potential of this technology.

2.2 Dual-radiator RICH

Contacts: Z.W. Zhao <zwzhao@jlab.org>, E. Cisbani <evaristo.cisbani@iss.infn.it>

The goal for this detector is to provide continuous $\geq 3\sigma$ hadron separation ($\pi/K/p$) from 2.5 to 50 GeV/ c . The design uses outward-reflecting mirrors (similar to LHCb or HERMES) to extend the momentum

coverage, in particular for the gas. A configuration with outward reflecting mirrors has the advantage of moving the focal-plane away from the beam and into the shadow of the barrel calorimeter, reducing backgrounds and requirements on the radiation hardness of the sensors, and allows light from the gas to reach the sensors without passing through the aerogel, which is a strong UV scatterer. The mirrors are divided into six sectors which greatly reduces the sensor area (Fig. 2.2.1) - which is the main cost driver for this type of detector. In fact, the total sensor area is determined essentially by the focal length of the mirror, which is the same for either inward or outward reflecting optics. In this study we benefited from the experience provided by several groups that have built similar devices in the past, and also by the CLAS12 RICH experience which is in progress [1, 2, 3].

Simulations were initially performed for a configuration using CF_4 gas, for which the current layout is optimized, but the study showed that C_2F_6 is a better match for $n=1.02$ aerogel in that it provides continuous coverage (more than $3\sigma \pi/K$ separation: Fig 2.1.4) without having to use the gas as a threshold device. The following key parameters of the RICH detectors were used in the Geant4 (GEMC) Monte Carlo simulation: i) device length 1.65 m; ii) aerogel radiator ($n(400 \text{ nm}) = 1.02$) thickness 4 cm; iii) gas (CF_4 or C_2F_6) tank length 1.6 m; iv) angular coverage $[5^\circ, 25^\circ]$; v) mirror radius 2.8 m, tilt angle 26.65 degrees, vi) detector plane, spherical shape, area of about 8500 cm^2 per sector. The magnetic field used for the simulation is the JLab detector field design at 3T central field.

Figure 2.2.1 shows a sketch of the detector, composed of 6 sectors each covering 60° in azimuthal angle.

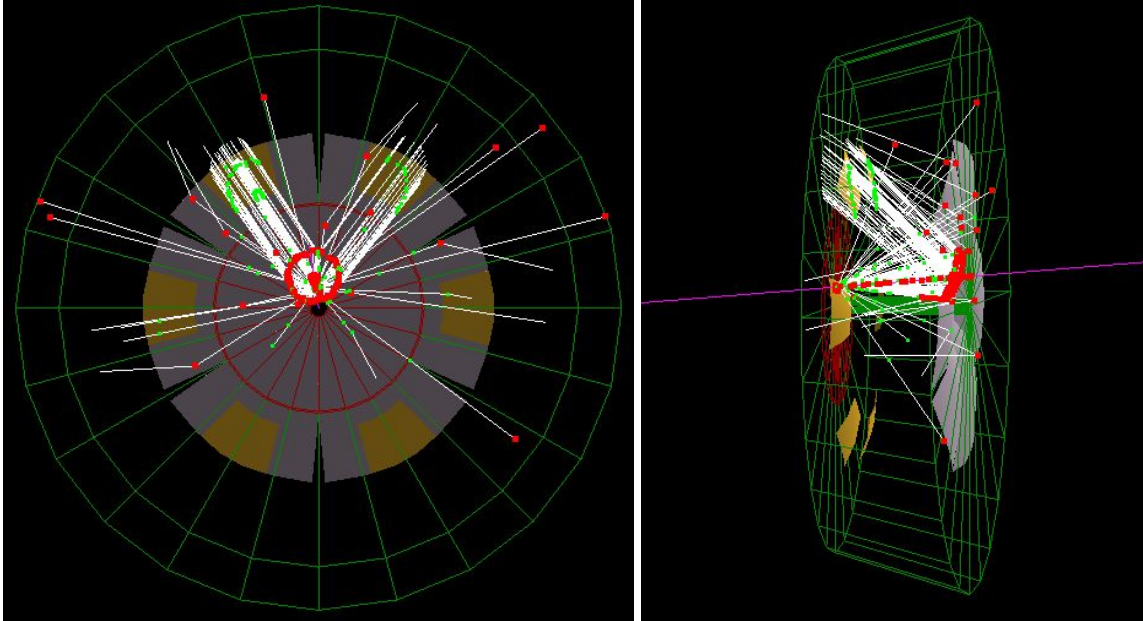


Figure 2.2.1 Sketch of the detector in GEMC simulation. (left panel) view from the back, in red is the aerogel radiator; in green is the gas tank; the six mirror sectors are in grey; the six photodetector sectors in yellow, (right panel) lateral view.

2.2.1 Dual-radiator RICH: Simulation and Performance

To analyze the simulated data and to estimate the performances in terms of error contributions to the

Cherenkov ring resolution and the particle separation power, we have implemented the indirect ray tracing algorithm used by the HERMES experiment [1].

In Fig. 2.2.2 (upper panel) the contributions to the single p.e. error as a function of the track polar angle are shown; as the detector is embedded in magnetic field, the track bending is a sizable error source for the gas Cherenkov ring. In Fig 2.2.2 (lower panel) the separation powers are shown for the CF_4 gas configuration; an analogous plot is shown for the much better C_2F_6 case in Fig 2.1.4.

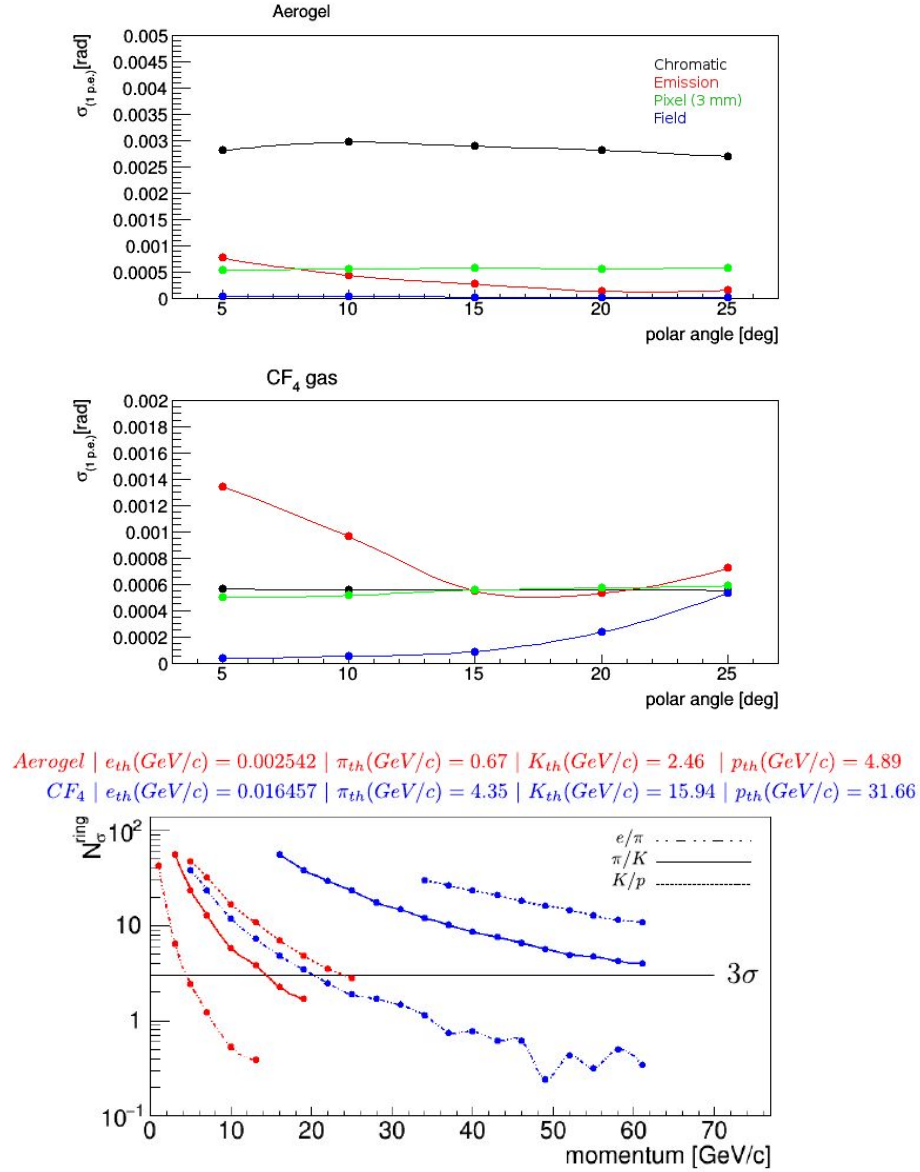


Figure 2.2.2 (upper panel) Single p.e. error sources, for a 30 GeV/c pion, assuming a pixel size of 3 mm. (lower panel) Particle separation power for tracks with 15° polar angle, using CF_4 as a gas radiator (see Figure 2.1.4 for C_2F_6).

2.2.2 FY16 Progress and Achievements

We have achieved the following results:

- A design of the dual RICH detector in the GEMC framework; in this context the MC has been tuned on the basis of the existing literature [1,2,3]. The MC includes all the important optical properties of the materials (*i.e.*, Rayleigh scattering, delta electrons, etc).
- The spectrum of the aerogel photons has been cut below a wavelength of 300 nm by software, using a typical photodetector quantum efficiency function. The dual configuration most likely will need a separation of the aerogel from the gas by using an acrylic material shield, this will also filter the aerogel photons at low wavelength. The shielded configuration is under study in the GEMC framework.
- The Indirect Ray Tracing algorithm [1] has been used for the evaluation of the particle separation performances and for the characterization of the detector.
- A study of the position of the real focal plane as a function of the mirror parameters, has lead to a spherical-like surface for the detector as a good “simple” option for reducing the photon emission uncertainty.
- A contribution concerning the dual-radiator RICH and the modular RICH has been submitted and accepted as poster in RICH 2016 (proceedings in NIMA) [4].

2.2.3 Proposed Dual-radiator RICH activities

2.2.3.1 Software: Simulation

We intend to proceed with the analysis of the detector performances and its optimization by:

FY17:

- A more detailed study of the background, also adding the acrylic shield mentioned above.
- Study and implementation of existing (or new) reconstruction algorithms to be compared with the IRT algorithm. Following this path, we expect to reduce some error sources (*i.e.* emission error, magnetic field error) by improved, dedicated algorithms (MC based maximum likelihood, iterative algorithms).
- GEMC-based digitalization of the photodetector (also useful for the definition of the photon detector baseline), optimal pixel shape to fit with a non planar surface.
- Formulation of requirements on the EIC detector for optimal RICH performance (magnetic field, track reconstruction, etc)
- Simulation of the feasibility of a compact version of the dual-radiator RICH to better fit the BNL versions of the EIC detector, and evaluate the performance using the current BNL parameters for the magnetic field.

FY18:

- Study of the physical background (*i.e.* assuming channel of physics of particular interest in the EIC context) on the basis of interaction and synergy with the full EIC detector layout.
- Evaluation of the dual-radiator RICH performances in such an extended (physics) context.
- Configuration and simulation of a small scale version of the dual-radiator RICH in view of

validating the GEMC simulation with a prototype.

2.2.3.2 Hardware: toward a prototype

To further validate the MC we shall consider a first, small scale prototype to investigate, at least, the effect of the magnetic field and the correlated photon detector response.

Our aim is to use as much as possible material borrowed from within the collaboration and to maximize potential synergy with other JLab development, such as the CLAS12 RICH.

FY17:

Both activities below are synergistic with the Photosensors and Electronics FY17 activities as described in Sect. 4.4.

- Identification of baseline candidates as photon detector: as we have to deal with magnetic field, the possible candidates are MCP-PMT, SiPM (both on the market) and LAPPD.
- Study and definition of a small scale prototype, figuring out how to maximize the opportunity of synergy with current JLab and collaboration developments and the reuse of existing components.

FY18:

- Realization of the prototype, beam test, data analysis and MC validation (possible iteration).

2.2.4 Dual-radiator RICH R&D Deliverables

FY17:

- Preliminary conceptual design report, assessment by Monte Carlo analysis
- Definition of a small scale prototype

References

[1] Akopov, Norair, et al. "The HERMES dual-radiator ring imaging Cherenkov detector." *Nuclear Instruments and Methods in Physics Research Section A: Accelerators, Spectrometers, Detectors and Associated Equipment* 479.2 (2002): 511-530.

[2] Adinolfi, M., et al. "Performance of the LHCb RICH detector at the LHC." *The European Physical Journal C* 73.5 (2013): 1-17; Alves Jr, A. Augusto, et al. "The LHCb detector at the LHC." *Journal of instrumentation* 3.08 (2008): S08005; Nobrega, R. Antunes, et al. "LHCb reoptimized detector design and performance: Technical Design Report." (2003): x-127.

[3] Anefalos Pereira., et al. "Test of the CLAS12 RICH large scale prototype in the direct proximity focusing configuration.", *Eur. Phys. J. A* **52** (2016).

[4] A. Del Dotto for the EIC PID consortium, "Design and R&D of RICH detectors for EIC experiments" accepted in poster section of RICH 2016, 9th International Workshop on Ring Imaging Cherenkov Detectors; (proceedings will be published in NIMA).

2.3 Modular Aerogel RICH (mRICH)

Contacts: H. van Hecke <hubert@lanl.gov>, X. He <xhe@gsu.edu>

The modular aerogel RICH is designed for hadron identification covering a momentum range of 3-10 GeV/c. Silica aerogel has been used for decades in threshold Cherenkov counters for high energy physics experiment and has recently been used as radiator material for RICH detectors for the HERMES, LHCb, AMS, Belle experiments [1-4], and for the CLAS12 experiment. This R&D has been benefiting from having in house expertise acquired from CLAS12 RICH [5].

The optical properties of aerogel are crucial parameters for the performance of mRICH. For instance, any angular dispersion of the emitted photons affects the precision of the Cherenkov angle measurements. In addition, a high transparency (transmittance) and a proper refractive index are required in order to collect a sufficient number of photons for a reliable ring reconstruction.

The design features of the mRICH are shown in Figure 2.3.1. The main components of the modular design include: (a) the aerogel block at the front (characteristic dimension: 10cm x 10cm x 3cm and $n = 1.01 - 1.05$), (b) focusing Fresnel lens (for projecting Cherenkov ring image toward the central region of the photosensor plane), (c) high quality mirror set on the side walls, and (d) the photosensor plane.

The focus of this particular R&D is to systematically study the mRICH performance through simulation with realistic material properties of the aerogel block, fresnel lens and mirror configuration (i.e. tilting angle) and to verify the simulation results through prototyping and beam test. The performance of the mRICH in the EIC detector will also be studied.

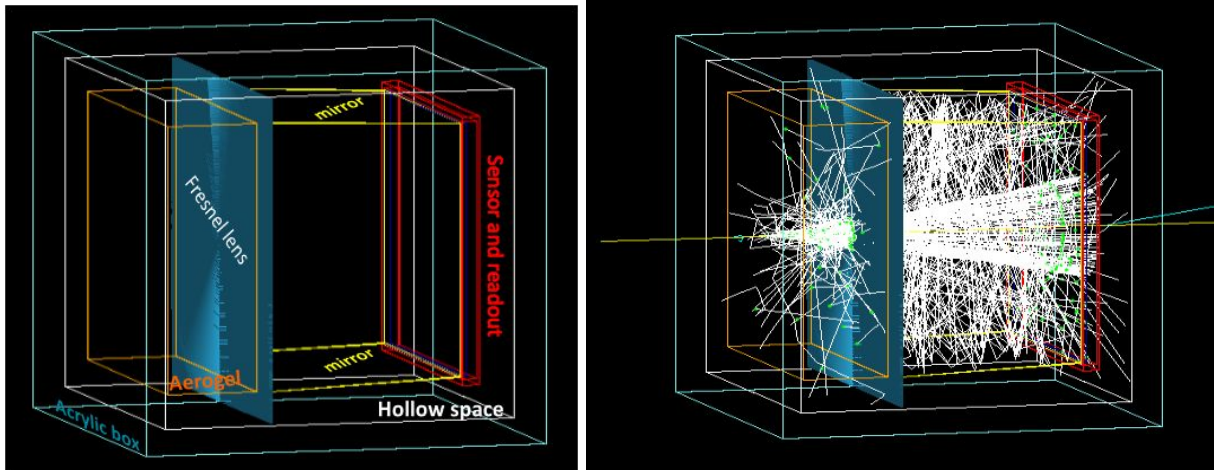


Figure 2.3.1 (Left) Modular RICH detector geometry in GEMC simulation. (Right) Event display from 9 GeV charged pions in GEMC simulation.

2.3.1 FY16 Progress and Achievements

The major achievement of the mRICH R&D includes: 1) The design and construction of the first prototype; 2) The prototype beam test at Fermilab; and 3) the improved and realistic Geant4 simulation using the GEMC framework.

- **Prototype and Beam Test**

The first beam test of the mRICH prototype was successfully performed at Fermi National Accelerator Laboratory from April 18 to 29, 2016. The detector components were designed and built with GSU internal fundings. The readout was provided by the INFN group led by Marco Contabrigio. The photos in Figure 2.3.2 show the detector setup (left) in the M6 test beamline at Fermilab and the control room (right).

The mRICH was mounted at the center of a supporting structure frame. Figure 2.3.3 shows the detector holder box (left) with HV, LV and optical connectors mounted on the backplane. Also shown in Figure 2.3.3 (right) is the stuffed holder box with the readout electronics provided by the INFN group. The beam incident direction was provided by two sets of hodoscopes which were constructed with 1cm x 1cm x 20cm scintillator rods as shown in Figure 2.3.4.

There are two major lessons learned from the first beam test: First, it is important to decouple the optical section of the holder-box from the readout electronics section in order to maintain the light tightness of the optical section and to avoid overheating the readout electronics. Second, the photosensors must have pixel size of 3mm x 3mm or smaller for hadron identification capability.

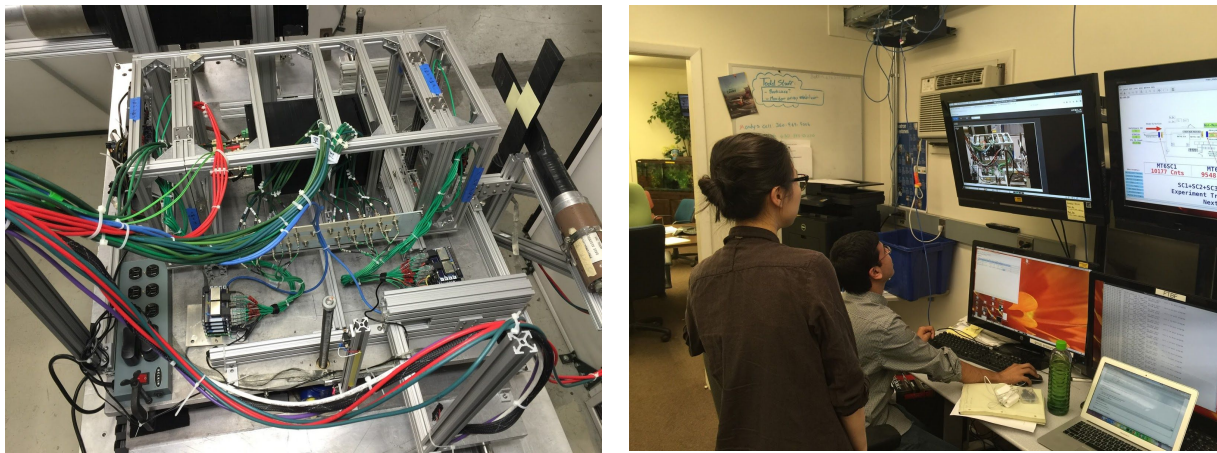


Figure 2.3.2 (Left) mRICH detector setup in the M6 test beamline at Fermilab. (Right) Control room operation for adjusting detector alignment with beam direction.

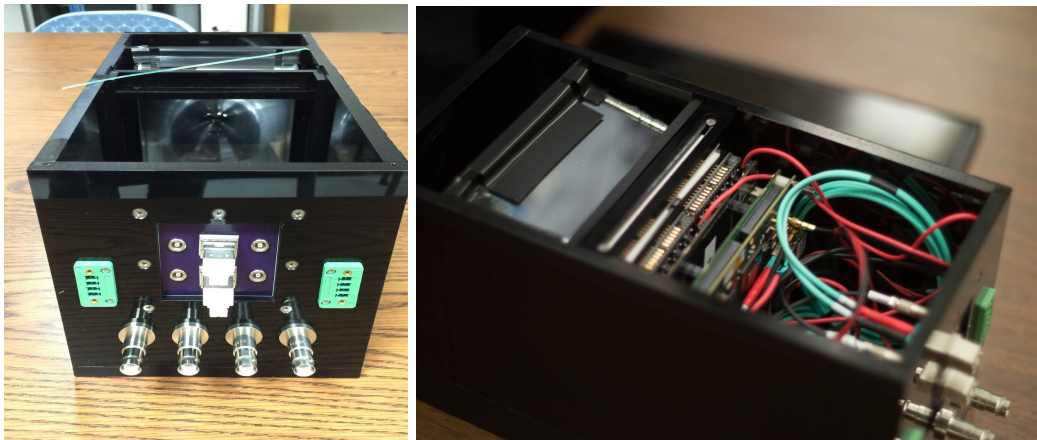


Figure 2.3.3 (Left) mRICH detector holder-box. (Right) Readout electronics mounted at the end section of the holder-box.

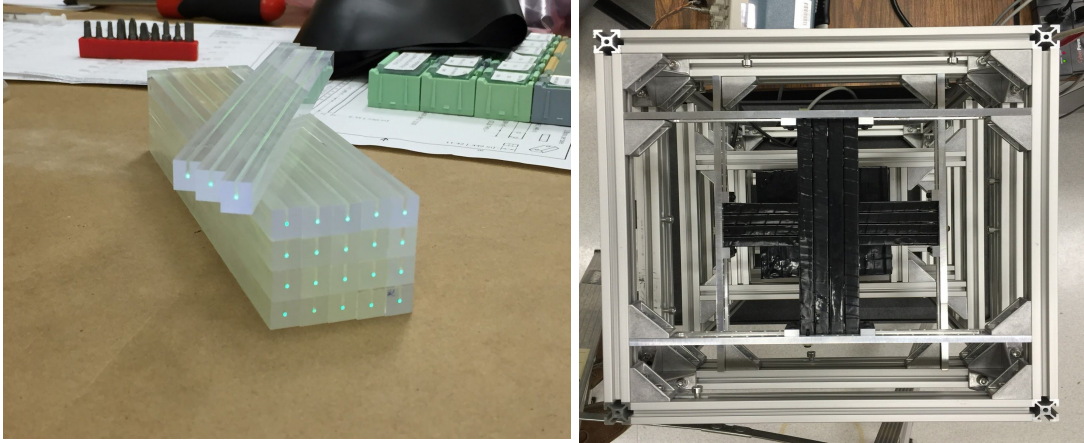


Figure 2.3.4 (Left) 1cm x 1cm x 20cm scintillator rods with embedded wavelength shifting fibers. (Right) Front view of the beam hodoscope mounted in front of the mRICH detector box.

- **Simulation Studies and Data Comparison**

Extensive simulations have been performed over the course of FY16 using the GEMC framework. The improvement includes the added Rayleigh scattering for the Aerogel block, updated geometry, material, and optical property of Fresnel lens, and updated size of photon sensor plane. The dimensions of the mRICH components are listed in Table 2.3.1.

As an example, Fig. 2.3.5 shows the Cherenkov ring image from the 120 GeV primary proton beam in comparison with the simulated results. It turns out that the 120-GeV narrow (~2-mm wide) primary beam at the Fermilab Test Beam Facility is quite useful for aligning the detector position. In this case, the beam was incident at the lower left quadrant (as marked with the white asterisk), and the generated Cherenkov ring was shifted by the Fresnel lens toward the center of the sensor plane. Detailed data analysis is currently ongoing, which mainly include (but not limited to): (a) 120 GeV proton beam incident on different quadrants; (b) Image studies with 4 and 8 GeV pion beams; (c) Comparison of Cherenkov ring images generated from the 3-cm aerogel block and a 2-cm aerogel block.

Table 2.3.1 Properties of the mRICH Detector Components.

Aerogel	3.3cm thick Refractive index $n = 1.03$
Fresnel lens	262 grooves Focal length $f = 7.62\text{cm}$
Mirror set	On four sides: top, bottom, right, and left
Photon sensor	Sensitive area = $9.6\text{cm} \times 9.6\text{cm}$

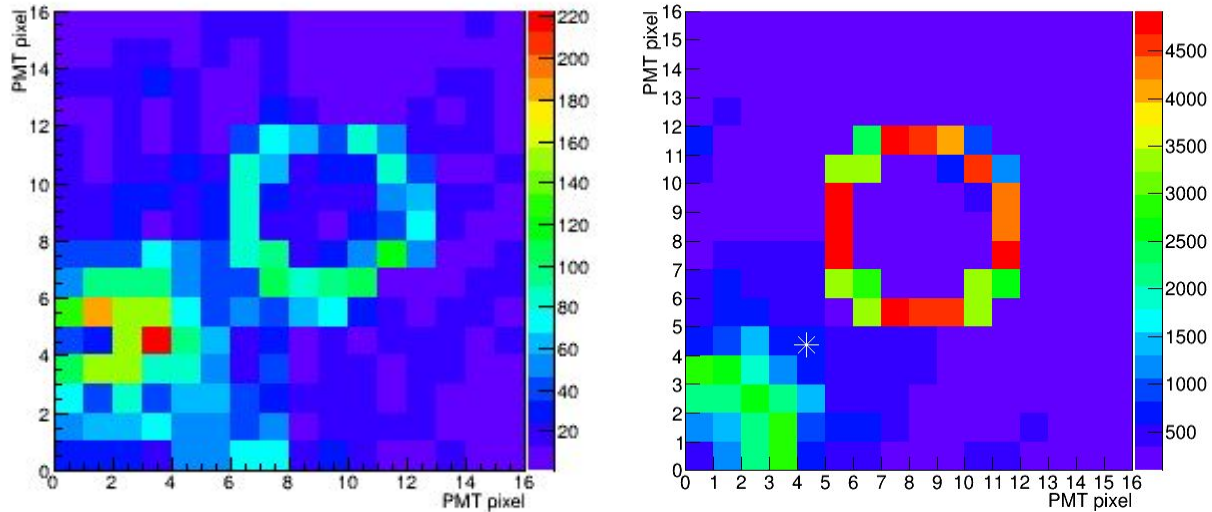


Figure 2.3.5 Comparison of beam test result (left) to simulation result (right) from a 120 GeV proton beam. The beam hit in the lower-left quadrant (marked with asterisk) of the mRICH and the produced Cherenkov ring was focused to the center of the sensor plane by the fresnel lens.

2.3.2 Proposed mRICH R&D Activities

The proposed activities include: 1) analyzing the first prototype beam test data and publishing the results; 2) improving the mRICH holder box design with flexible readout plane integration and preparing for the second beam test with 3-mm pixel-size sensors; and 3) continuing mRICH simulation study with focuses on realistic EIC detector configurations.

FY17:

- Analyzing the first mRICH beam test data and publishing the results.
- Improving the detector design to decouple the optical section and the readout electronics section.
- Acquiring photosensors with smaller pixel size (3 mm x 3mm or smaller), preparing for, and carrying out a second beam test.
- Systematic simulation studies of Fresnel lens to optimize the Cherenkov ring image on the sensor plane.

FY18:

- Performing systematic mRICH simulation studies within the EIC detector configuration.

2.3.3 mRICH R&D Deliverables

FY17:

- Publication of the first-beam test mRICH results.
- Designing and building the second mRICH detector.
- Performing a second mRICH beam test at Fermilab.

FY18:

- Report on results from the second beam time.

References

- [1] F. Muheim, Nuclear Instruments and Methods in Physics Research Section A **639**, 11 (2011).
- [2] S. Iwata et al., International Conference on Technology and Instrumentation in Particle Physics 2011: Proceedings of the 2nd International Conference on Technology and Instrumentation in Particle Physics, Physics Procedia **37**, 2012, 820.
- [3] T.A Shibata, Nuclear Instruments and Methods in Physics Research A **766**, 267 (2014).
- [4] F. Giovacchini, Nuclear Instruments and Methods in Physics Research Section A **766**, 57 (2014).
- [5] M. Contalbrigo et al., Nuclear Instruments and Methods in Physics Research Section A **766**, 22 (2016).

2.4 DIRC

Contacts: G. Kalicy <gkalicy@jlab.org>, J. Schwiening <J.Schwiening@gsi.de>

A radially-compact detector based on the DIRC (Detection of Internally Reflected Cherenkov light) principle is a very attractive solution for EIC, providing particle identification (e/π , π/K , K/p) over a wide momentum range. The DIRC detector is a special kind of RICH counter using rectangular-shaped radiators made of synthetic fused silica that are utilized also as light guides to transport Cherenkov photons to an expansion volume, where they are recorded by an array of photon sensors. During the photon transport the emission angle of Cherenkov photons with respect to the particle track is maintained and can be reconstructed from the measured parameters. DIRC detectors are inherently 3D devices, measuring the image location on the detector surface (x , y) and the time of arrival of each photon (t).

The expected PID performance of the DIRC is determined by the resolution in θ_c , the polar opening angle of Cherenkov light emitted from the particle traversing the detector. The angle θ_c is defined as $\cos\theta_c = 1/(n(\lambda)\beta)$, where $\beta = v/c$, v is the particle velocity and $n(\lambda)$ is the index of refraction of the material. In a dispersive medium the latter is a function of λ , the wavelength of the Cherenkov photon.

The uncertainty of the Cherenkov angle for a particle track, σ_c^{track} , behaves in first approximation as

$$(\sigma_c^{track})^2 = (\sigma_c^{photon}/\sqrt{N_{p.e.}})^2 + (\sigma^{track})^2, \quad (2.4.1)$$

where $N_{p.e.}$ is the number of detected photoelectrons and σ_c^{photon} is the single-photon Cherenkov angle resolution. The last term, σ^{track} , is the uncertainty of the track direction in the DIRC, dominated by multiple scattering and the resolution of the tracking detectors.

Figure 2.4.1 shows how the maximum momentum goal for π/K and e/π separation translated into the required Cherenkov angle resolution. In an EIC, the pion background for kaons varies with reaction channel and kinematics, but in general a 3σ criterion is relevant. Achieving 3σ separation using fused silica radiator bars would require a Cherenkov angle resolution of 1.3 mrad at 5 GeV/c and 1.0 mrad at 6 GeV/c. Achieving this resolution assumes that the central tracker will be able to provide an angular resolution at the sub-mrad level (*i.e.*, comparable to the CLAS12 forward detector). The R&D undertaken by the EIC PID consortium achieved the goal of showing feasibility of a high-performance DIRC that would extend the momentum coverage well beyond state-of-the-art allowing 3σ separation of π/K up to 6

GeV/c, e/K up to 6 GeV/c, e/π up to 1.7 GeV/c, and K/p up to 10 GeV/c.

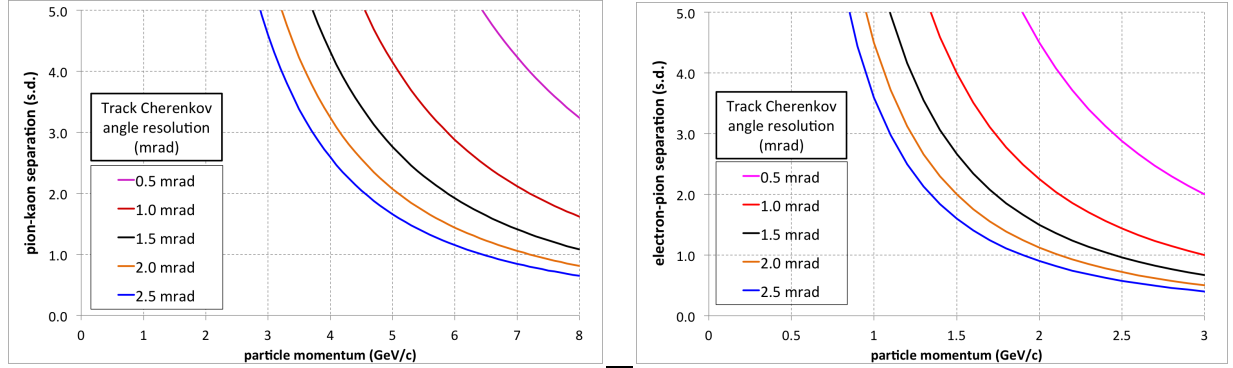


Figure 2.4.1: π/K separation (left) and e/π separation (right) in the DIRC in units of standard deviations (s.d.) as function of particle momentum for different values of the track Cherenkov angle resolution σ_c^{track} . A track Cherenkov angle resolution of 1 mrad is required to achieve 3 s.d. π/K separation at 6 GeV/c and 3 s.d. e/π separation at 1.7 GeV/c.

2.4.1 High-Performance DIRC Simulation and Performance

The baseline design, implemented in a Geant4 simulation, is shown in Fig. 2.4.2a. The radiators are synthetic fused silica bars, each 4200 mm long, with a cross-section of 17 mm x 32 mm. 11 such bars are placed side-by-side, separated by a small air gap, into a bar box. The 16 bar boxes are arranged in a barrel with a radius of 1 m around the beam line. Mirrors are attached to one end of each bar. On the readout end, where photons exit the bar, a special 3-layer spherical lens, which will be described further, is attached to each bar. The other side of the 3-layer lens is coupled to a prism that serves as an expansion volume. A zoom on the bar box, lenses and prism section is shown on a right side of Fig. 2.4.2b, together with a breakdown of each layer of the lens and photos of a prototype lens. The prism is made of fused silica, has a 38° opening angle, and the dimensions 285 mm x 390 mm x 300 mm. The detector plane of each prism is covered by 2 mm x 2 mm pixels for a total of about 450k channels to record the location and arrival time of the Cherenkov photons.

A key component to reach the required performance is a special 3-layer spherical compound lens. Schematic and photos of a prototype of the 3-layer lens, tested in 2015, is shown in Fig. 2.4.2c. It contains a layer of high-refractive index material Lanthanum crown glass (NLaK33), sandwiched between two layers of synthetic fused silica. The two radii of the 3-layer lens were optimized to remove aberrations present in standard lenses by first defocusing and then defocusing transmitted photons to create a flat focal plane, matching the geometry of the prism expansion volume.

The figures of merit of the high-performance DIRC design, evaluated using the Geant4 simulation, are shown in Fig 2.4.3: The number of measured photons per track and the Cherenkov angle resolution per photon. The Cherenkov angle resolution was obtained using the geometric reconstruction, similar to the one used for BaBar DIRC. It transforms the known spatial positions of the bar through which the track passed and the pixel with a detected photon into the Cherenkov coordinate system. The direction of a

detected photon is approximated by the three-dimensional vector between the center of the bar and the center of the pixel. The full simulation is used to calculate these photon direction vectors for every possible bar-pixel path and stores them in so-called “Look-up” tables.

The average number of photoelectrons per track (photon yield) is shown as a function of the particle track polar angle in Fig. 2.4.3a. It is worth noting the large yield around 90° , where traditional lenses with an air gap would provide almost zero yield. The reconstructed single photon Cherenkov angle resolution (SPR), as a function of the particle track polar angle is shown in Fig. 2.4.3b. Both SPR and photon yield are used to calculate track Cherenkov angle resolution using equation 2.4.1. The simulation showed how critical the resolution of the central tracker is for achieving the optimal PID performance. To reach 1 mrad track Cherenkov angle resolution by High-performance DIRC the tracking system resolution has to be at the level of 0.5 mrad.

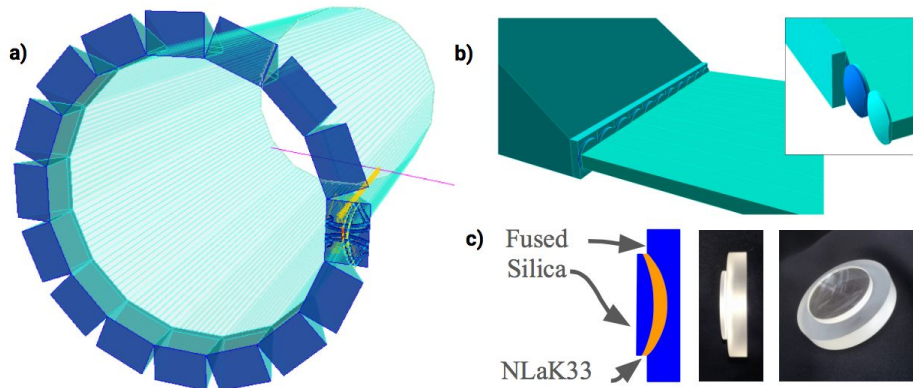


Figure 2.4.2: a) Geant4 geometry for the simulation of the high-performance DIRC. b) The fused silica prism expansion volume, a row of spherical three-layer lenses with high index of refraction (no air gaps) and the radiator bars. The insert shows the individual lenses and layers of the spherical lens system. c) Schematic and photos of the 3-layer lens prototype.

The required sensor pixel size and its influence on the single photon resolution was studied with Geant4 simulations. A pixel size of 2-3 mm would be a good choice for the high-performance DIRC design if the Cherenkov angle is reconstructed using geometrical method. This is about half the size of the pixels of standard square Microchannel Plate Photomultiplier Tubes (MCP-PMTs) from PHOTONIS or Hamamatsu. Reducing the pixel size is not technically challenging for the manufacturers and PHOTONIS already has an available sensor, called XP85122, with 32 x 32 pixels and a 1.6 mm pixel pitch. However, the small pixel size will increase the channel density and cost of the readout electronics.

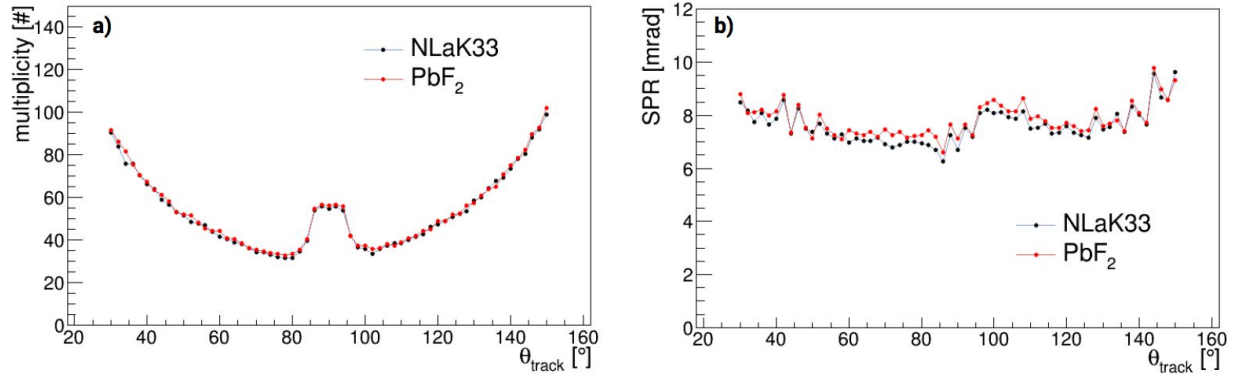


Figure 2.4.3: Photon yield (a) and single photon Cherenkov angle resolution (b) for two versions of the 3-layer lens implemented in the high-performance DIRC. One is using NLaK33, the other is using PbF₂ as the middle, high-refractive index layer.

2.4.2 FY16 Progress and Achievements

2.4.2.1 Hardware: Development and Validation of the 3-layer Spherical Lens

CERN Beam Test

Experimental validation for the properties of the 3-layer lens is crucial for the DIRC in the EIC R&D program. Pictures of the prototype lens are shown in Fig. 2.4.2c. Not all of the other components of the high-performance DIRC baseline design are available yet (such as sensors with small pixels, fast readout electronics, full-size radiators, etc.). However, the validation of the simulation package, used to optimize the design and to determine the performance, can be done by simulating key components in a geometry corresponding to the currently available detector prototypes, and by comparing the results to test beam data. Here, the most important item is the special 3-layer lens.

The PANDA DIRC group provided an opportunity to evaluate the performance of the 3-layer lens in a real particle beam experiment. The modular design of the PANDA Barrel DIRC prototype allowed for the easy exchange of several components between measurements to test their impact on the prototype performance. The EIC DIRC simulation package was used for designing the prototype, monitoring the measurements, and analyzing the data. Several different focusing options were tested during the 2015 test beam campaign at CERN. Because of the larger pixel size of the MCP-PMTs used in the test beam (6.5mm pixel pitch), the different length of the bar and size of the prism, the results from this test beam are not expected to agree with the performance predicted for the high-performance DIRC.

The reconstructed photon yield and SPR are shown as a function of the track polar angle, and compared to simulation, in Fig. 2.4.4 for the configuration with the narrow bar radiator and the 3-layer spherical lens. The simulation describes the data within the *rms* of the distributions. The number of Cherenkov photons from the beam data ranges from 12 to 80 and the SPR is between 8 mrad and 12 mrad. For polar angles below 40° the simulation overestimates the photon yield by about 10%, which may be an indication of an

incorrect mirror reflectivity value used in the simulation. Around 90° the photon yield in the beam data is more than 30% below the simulation. This difference is most likely due to the way the MCP-PMTs were selected for this beam test. The newer units with the higher gain were placed into the columns on the side of the prism to get the best efficiency for the angles below 60° , which is the most difficult range in terms of PID in PANDA. The older units were placed in the column, where they only affect the ring image of polar angles in the range of $80\text{--}100^\circ$, a less demanding region for PANDA.

The single photon Cherenkov angle resolution for the same data set (narrow bar and the 3-layer spherical lens for tagged protons at 7 GeV/c momentum) is shown in Fig. 2.4.4b. The beam data and simulation are consistent within the RMS of the distributions for the forward and backward angles. Again, the beam data performance is somewhat worse than simulation for polar angles around 90° and the less efficient MCP-PMT coverage contributes to this effect as well. The poorer timing resolution and the additional background in the data particularly affects this polar angle region because the shape of the combinatorial background is especially complicated due to many overlapping ambiguities. This makes the time cut less efficient, the fits to the θ_c distributions less stable and the widths larger.

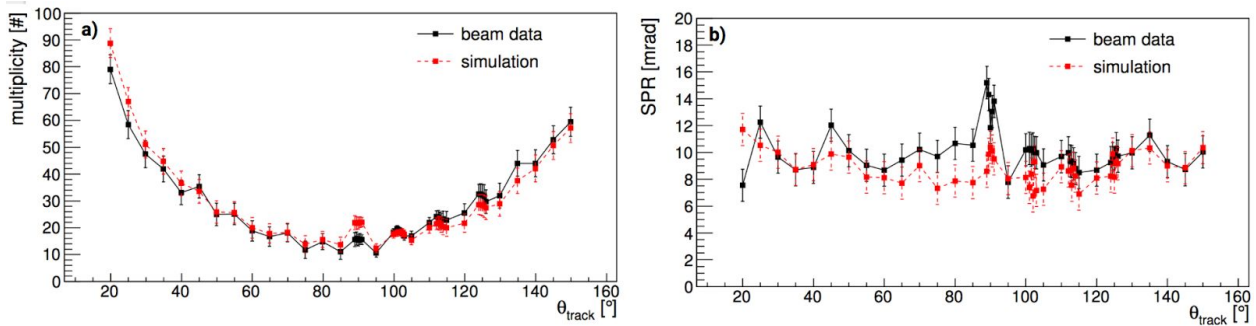


Figure 2.4.4: Results from the 2015 CERN beam test: Photon yield (a) and SPR (b) as a function of the track polar angle for the narrow bar and the 3-layer spherical lens for tagged protons at 7 GeV/c beam momentum in data (black) and Geant simulation (red). The error bars correspond to the *rms* of the distribution in each bin.

Radiation Hardness Test at CUA



Figure 2.4.5: a) Irradiated samples in X-ray setup at CUA. b) 3-layer lens in the transmission measurement setup. c) Transmission measurement before irradiation of synthetic fused silica plate (black) and 3-layer lens (red).

The determination of the radiation hardness of materials is an important aspect of the EIC R&D. Synthetic fused silica, which is used for most of the optical components in all DIRC systems, was already

extensively tested in the BaBar and PANDA experiments and proved to be radiation hard. However, the middle layer of the 3-layer lens is made of a high-refractive-index lanthanum crown glass, NLaK33, which has yet to be tested for radiation hardness. The irradiation is being performed at Catholic University of America in an X-ray setup, shown in Fig. 2.4.5a, with energies up to 160 keV. The dose will be accumulated in small steps, delivering a dose of 0.01-0.1 krad at a time, depending on the observed result. Between each step the transmission properties of the lens and a pure NLaK33 sample will be measured in a setup, shown in Fig. 2.4.5b with a reproducibility of 0.2% to quantify the impact of the radiation. A thin synthetic fused silica plate, which is never placed in the X-ray setup, is used as a reference for the transmission measurement. The X-ray setup is already commissioned and is currently being calibrated. A first example plot showing a comparison of the transmission of fused silica and the 3-layer lens before irradiation is shown in Fig. 2.4.5c. Results regarding the radiation hardness of the 3-layer lens and the pure NLaK33 sample are expected in July.

Meanwhile, possible alternatives to NLaK33 for the next iteration of the 3-layer lens prototype are being investigated. However, most optical glasses with a high refractive index, especially if they are radiation-hard, cut off UV photons at around 400 nm. Lead fluoride (PbF_2) has a high refractive index ($n=1.77$), is radiation hard, and has a cut off at 300 nm. With this material a flat focal plane at a required distance can be achieved. Investigation of PbF_2 as a lens material is in progress and to show if this material is mechanically usable for lens production. Simulation studies were already performed and are shown in red in Fig. 2.4.3. The final design for the PbF_2 version of the 3-layer lens has to be optimized for best focussing but already this early version has a comparable performance to the 3-layer lens with NLaK33 (black points on Fig. 2.4.3).

Mapping of the Focal Plane at ODU

A special setup was designed and built at the Old Dominion University laser lab to measure the shape of the focal plane of the 3-layer lens. The schematic of the setup is shown in Fig. 2.4.6. The lens is placed on a rotating stage and rotated through two parallel laser beams. The intersection point of the two laser beams determined the focal length. The lens was placed inside a 30 x 40 x 60 cm³ glass container filled with mineral oil (with a refractive index very close to fused silica) to simulate the focusing behavior of a lens placed between the bar and the prism. The 3-layer lens is supported in a special 3D-printed holder that makes it possible to map out the focal plane in all three dimensions, which will be particularly important for comparing spherical and cylindrical lens designs. The setup was commissioned and first measurement were performed. However, due to the need to purchase a new laser with a better beam profile, the final results are delayed and expected in July.

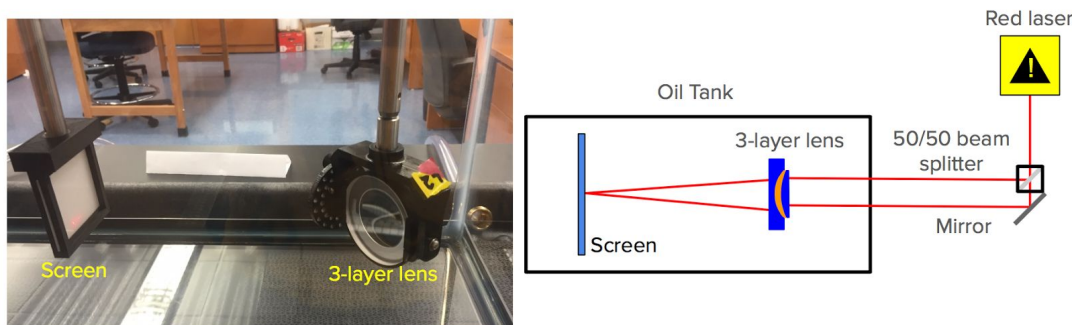


Figure 2.4.6 Photo (left) and schematic (right) of the setup at ODU to map the shape of the 3-layer lens focal plane.

2.4.2.2 Software: Simulation

Development of the Time-Based Imaging Method

This new reconstruction method was initially primarily motivated by the possible use of a wide plate instead of a narrow bar as the radiator. The geometrical reconstruction approach cannot be used in that case since the fundamental assumption that the photon exits from the center of the radiator is no longer valid. This alternative algorithm, developed for the wide plates, can also be used for narrow bars. The time-based imaging method is based on the approach used by the Belle II time-of-propagation (TOP) counter. The basic concept is that the measured arrival time of Cherenkov photons in each event is compared to the expected photon arrival time for every pixel, track momentum and location, and for every particle hypothesis, yielding the PID likelihoods.

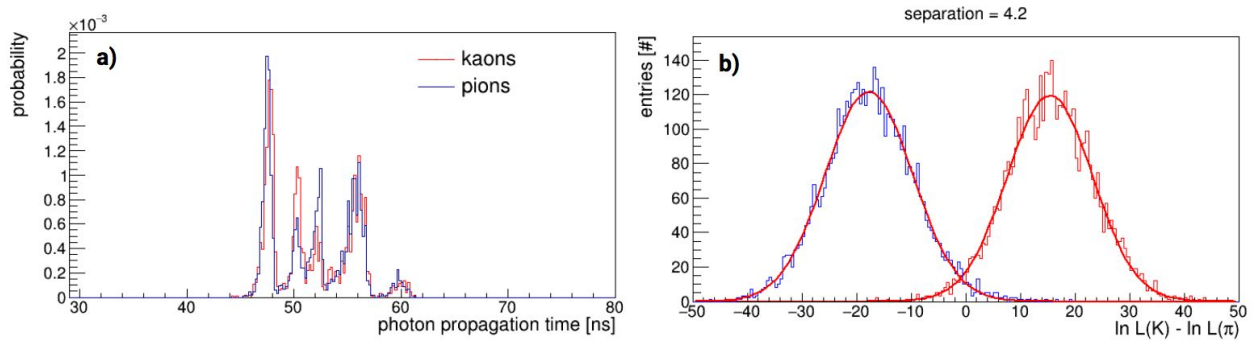


Figure 2.4.7 Example for the time-based imaging of the high-performance DIRC geometry with narrow bar radiators and 3-layer spherical lenses: photon arrival time for charged pions and kaons for a selected MCP-PMT pixel (a) and log-likelihood difference for kaon and pion hypotheses for a sample of 6 GeV/c pions and kaons at 30° polar angle (b). The π/K separation power extracted from the Gaussian fits is 4.2 standard deviations.

The full detector simulation is used to generate a large number of tracks with the observed momentum, location, and charge of the particle. The arrival time of the Cherenkov photons produced by e , μ , π , K , and p is recorded for every pixel and stored in an array of normalized histograms to produce probability density functions (PDF). An example for one MCP-PMT pixel is shown in Fig. 2.4.7a. The resolution of the detected time was chosen to be 100 ps, the expected single photon timing resolution for the high-performance DIRC. For a given track the observed photon arrival time for each hit pixel is compared to the histogram array to calculate the time-based likelihood for the photons to originate from a given particle hypothesis. Figure 2.4.7b shows an example of the log-likelihood difference for kaon and pion hypotheses for a sample of 6 GeV/c pions and kaons at 30° polar angle. The π/K separation, calculated as the difference of the two mean values of the fitted Gaussians divided by the average width, corresponds to 4.2 standard deviations in this case. This first example of applying the time-based imaging shows that it is potentially more powerful than the geometrical reconstruction due to the optimum use of all observables. Nevertheless, a more detailed study for the full phase space and an optimization of the algorithm, as well as the implementation of an analytical approach to calculating the PDFs, are still required. One more test beam at the CERN PS may be possible in FY17. It would be dedicated to the validation of the time-based

reconstruction method with a wide plate. The EIC DIRC group would contribute with the new cylindrical 3-layer lens and take an active role in the data taking and analysis.

2.4.3 Proposed DIRC R&D Activities

Synergetic Activities Supported by External Funding

The synergy with the PANDA Barrel DIRC project not only provided access to the prototype and the CERN test beam campaign in 2015 but includes several planned mid- and long-term contributions from the GSI DIRC group to the EIC DIRC project. With the submission of the PANDA Barrel DIRC TDR, scheduled for the fall of 2016, the activity focus of the GSI DIRC group will shift to the mechanical design and the R&D for the detector assembly. Both activities are relevant to the EIC DIRC effort.

All major mechanical components of the PANDA Barrel DIRC are expected to be built from aluminum alloy and Carbon-Fiber-Reinforced Polymer (CFRP) to minimize the material budget and weight and to maximize the stiffness. The necessary R&D, to evaluate if outgassing from the CFRP components has a negative impact on the sensitive radiator surfaces, will provide valuable information for the EIC DIRC design, which is likely to follow the PANDA design closely. The finite element method (FEM) analysis of the Barrel DIRC design for PANDA can directly be applied to the EIC DIRC mechanical design since the expertise remains with the two engineers in the GSI DIRC group. The experience gained with handling DIRC bars or plates, with the gluing of bars and the assembly of bar boxes, and with the optical coupling of bar boxes to prims using silicone cookies, will also apply to the EIC DIRC.

After conclusion of the beam tests of the PANDA Barrel DIRC, components the prototype is expected to become available for use by the EIC DIRC effort during FY18 on the basis of a long-term loan or an in-kind contribution. The mechanical prototype structure, as well as one narrow bar, one wide plate, and a prism expansion volume, could be transported to the US for prototype beam tests at JLab or Fermilab. This would significantly reduce the financial investment required to set up a prototype for the test of lenses, sensors, and readout electronics with particle beams (this would be a deliverable in FY19).

Greg Kalicy was recently appointed as Assistant Professor at CUA. He will supervise the DIRC R&D post-doc. Catholic University has agreed to provide 50% FTE support for this postdoc. Greg is also joining the GlueX collaboration at JLab. Together with the GSI group, which also participates in GlueX, this creates a strong connection between this DIRC R&D program and the GlueX DIRC project. In particular this will provide physics-data tests of a mirror based expansion volume.

Proposed activities

FY 17

1. Simulation: Cost/performance optimization of bar/plate-based design , identify baseline design.
2. Simulation: Develop analytical version of time-based imaging.
3. Simulation: Determine optimum pixel size for sensors and system time resolution in the high-performance DIRC using time-based reconstruction.

4. Simulation: Investigate chromatic dispersion mitigation in context of different photocathode materials (for the narrow bar geometry).
5. Simulation: Investigate potential use of DIRC for event timing.
6. Hardware: Complete procurement of radiation-hard cylindrical 3-layer lens.
7. Hardware: Determine performance of cylindrical 3-layer lens in lab (and with particle beams, if available).

FY 18

1. Prototype: phase 0 of dedicated DIRC@EIC prototype development (modified PANDA DIRC prototype, possible in-kind contribution from GSI)
2. Develop initial mechanical design (possibly generic EIC detector, DIRC bar/prism boxes, etc).
3. Simulation: study reconstruction performance of the baseline design in the presence of backgrounds.
4. Start of the analysis of simulation and existing test beam data: comparison of DIRC designs, including (plate and bar) lens-based high-performance design with EV inside solenoid, FDIRC design, GlueX design, and other lens- and mirror-based designs with EV outside solenoid.

2.4.4 DIRC R&D Deliverables

FY17:

- Cost optimized baseline design of high-performance DIRC.
- Sensor and electronics requirements for high-performance DIRC using both geometrical and time-based reconstruction.
- Prototype of cylindrical 3-layer lens and its performance evaluation on test benches and in particle beam.
- Paper summarizing tests of the 3-layer lens.

FY18:

- First high-performance DIRC prototype.
- Mechanical design of high-performance DIRC.
- Evaluation of the impact of event- and track-related backgrounds on the PID performance.

2.5 High-resolution Time-of-Flight (TOF)

Contacts: M. Chiu <chiu@bnl.gov>, M. Grosse-Perdekamp <mgp@uiuc.edu>

High-resolution TOF provides a very attractive solution for PID covering the lower momenta range at the EIC, below the turn on threshold for gas RICH detectors. The R&D pursued here intends to push the state of the art of two technologies, MCP-PMT and mRPC, with an ultimate goal of 5 and 10 ps, respectively. Assuming a total resolution of 10 ps and a distance of 1 m, TOF could achieve 3σ separation for π/K and K/p of 3.5 and 6 GeV, respectively, which would be adequate for mid-rapidity PID. In the hadron going direction, where the TOF wall could be placed 3 m from the interaction point, the 3σ separation for π/K and K/p would be 6.5 and 11 GeV. Coupled with a dE/dx measurement from a TPC, TOF would also

provide electron identification up to several GeV. Besides PID, TOF enables bunch association, which is required since each bunch may have a different polarization.

TOF walls are also very compact. The TOF detectors proposed here are only about 2 cm thick and would fit in the available space of 10 cm in the ePHENIX barrel, even after a tilt to make them projective toward the IP. The cost of a mRPC-based TOF also makes them a very attractive option. Based on estimates from existing systems, a cost of about \$200K/m² is estimated for mRPC TOF. eRD14 is also pursuing TOF using LAPPD MCP-PMTs, which should be over an order of magnitude cheaper than MCP-PMTs from current vendors.

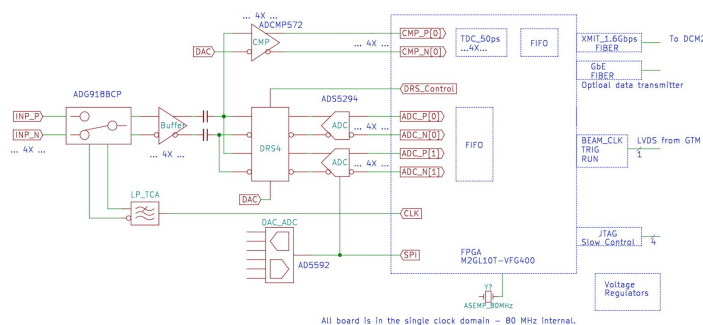
Within eRD14 (and previously eRD10), we have demonstrated that a resolution of ~18-25 ps is achievable with glass mRPCs by using thinner glass, and making smaller gas gaps as well as increasing the number of gaps. From a rate test in the COMPASS beamline, this performance seems to hold for fluxes up to 80 Hz/cm²/s, which should be adequate for the EIC.

To achieve even better resolution for the mRPC, we have proposed that one solution is to replace the glass with some other dielectric. The glass prototype we have built uses 210 μ m thick glass, and thinner glass gets much more expensive (in addition to starting to become flexible). Over the past year a 3D printed plastic version of the mRPC was made at UIUC (this may be one of the first 3D printed detectors). Initial testing of the 3D-printed mRPC was done at the FTBF, and it is now undergoing testing in a cosmic ray test stand at BNL. 3D printing is interesting to pursue since it may dramatically reduce the cost of production by saving on labor. It is also expected that 3D printing technology will continue to improve, so that 3D-printed mRPCs will improve along with them. We found that with the current state of the art, only 300 μ m gas gaps are possible; with smaller gaps, the plastic layers will have areas where they merge in the gaps. However, in the future as the technology improves we expect thinner gaps will become possible. Even with the lower performance from the 300 μ m gas gaps, a 3D printed mRPC could be a cost-effective solution for a lower performance TOF of ~100 ps resolution at the EIC.

In addition to the 3D printed mRPC, the first mylar mRPC ever was recently constructed at BNL. This mylar mRPC has 48 gas gaps (compared to 36 for the eRD14 UIUC glass prototype and 24 for the prototype made by Crispin Williams). Unfortunately, when tested, the mylar mRPC was found to suffer drastically from static charge build up. While signals could be seen, they were small and with very low efficiency. This should not have been surprising. On the triboelectric series, mylar has a large negative electron affinity of -40 nC/J. Fortunately, there may be a solution to the charging problem by using one of the many anti-static versions of mylar. An anti-static mylar mRPC is currently being built for testing by the ACU group during the summer at BNL. The anti-static mylar is usually made by a surface coating, achieving resistivities of $\sim 10^{12}$ Ω /cm². This is around the resistivity for the special high-rate glass mRPCs, so hopefully this anti-static mylar version can solve two problems. Interestingly, glass has a positive affinity of +25 nC/J on the triboelectric scale. This tendency for glass to resist electrons may be another factor that contributes to the rapid recombination of electronics and ions that is alleged by C. Williams.

One remaining impediment to a TOF system at the EIC is the availability of electronics capable of sub-10 ps timing resolution, that is low power, and that has enough trigger latency (around 4 μ s) for colliders.

Several ASICs have been proposed that would satisfy these requirements, such as the DRS5 and PSEC5. However, these ASICs will not be available for another 4-5 years. In any case, we are in dire need of more electronics for our testing. We currently use the DRS4 evaluation board for digitization, which only has 4 channels. This allows us to instrument only one cm wide set of strips per DRS4 eval board for timing studies, since we read out both ends of a strip and require two detectors.



When coupled with the preamps we have built over the past year, this DRS4 prototype board would enable us to instrument many channels. This would dramatically speed up our R&D since we could get data over a wider area of the detector. In addition, it will allow us to gain expertise in high speed low noise electronics, and really test whether electronics can be made to handle 10 ps detectors. In particular, one unsolved problem is the clock distribution. Since the detectors are spread far apart, a clock will need to be distributed synchronously over many meters with jitter much less than 10 ps, and we expect to devote much of our time looking into this problem. Besides the benefit for TOF at the EIC, the electronics R&D proposed here has also a lot of synergy with the high energy community, where they are looking into solving many of the same problems since 10 ps timing is required to separate the O(100) collisions that pile up within one crossing at the HL-LHC.

2.5.1 FY16 Progress and Achievements

During the past year we have tested the rate capability of a high resolution glass mRPC built at UIUC, and tentatively have concluded that it will have a resolution of at least 25 ps at a rate of 80 Hz/cm²/s. In addition, first consistent signals from the UIUC 3D-printed mRPC were measured in the test beam at the FTBF in April. The analysis of that data is on-going. The same system has been set up in a cosmic ray test stand at BNL, along with a small (6x6 cm²) silicon tracking system. We expect the final results from these studies for the 3D printed mRPC around the end of the summer.

Besides the 3D-printed mRPC, a mylar mRPC was built, using 125 um thick sheets of mylar. Initially, we believed it would be difficult to maintain uniform spacing with flexible mylar sheets, and there were complicated plans to tension the sheets from the ends, but we found that if the fishing line was spaced close enough together, and if they were run so that the lines lay right on top of each other, there was enough support to maintain good spacing. The spacing is shown in fig. 2.5.2 below for one stack of sheets. By going to mylar, we were able to have 12 gas gaps within the same 3mm thickness in 1 stack that was used in the glass mRPC.

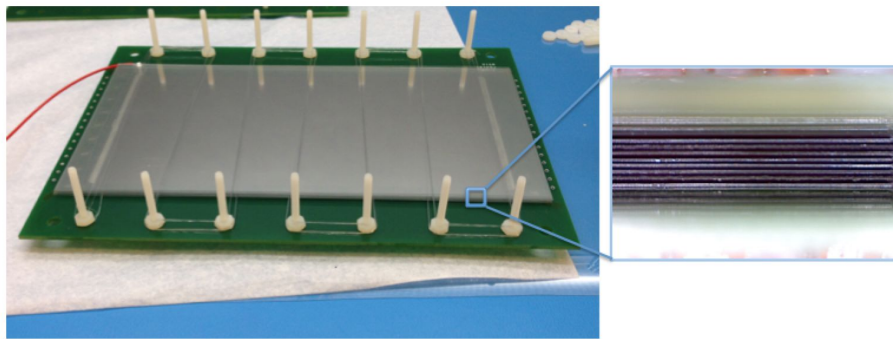


Fig. 2.5.2: Construction of a mylar mRPC. The uniformity of the spacing between the mylar sheets (gas gaps) are shown on the right.

Unfortunately, as mentioned previously, plain mylar suffers terribly from static charge up in a mRPC. The ACU group is currently building a small anti-static mylar mRPC to be tested to see if this solves the static charging problem.

During the test beam in April at the FTBF, we also tested the very first version of an LAPPD-style MCP-PMT with a 3mm thick UV fused silica window. To generate a larger signal, we coupled an additional 8mm thick fused silica window using Dow Corning 200 fluid, and tested it against a standard MCP-PMT. While this PMT was tested to have a TTS of 57 ps for single photoelectrons, we measured a timing resolution of about 36 ps from the beam particles. The MCP-PMT was just made in April by ANL, so this is an early result and we are still analyzing the data to understand better what is currently limiting the timing resolution.

In addition to the above, Garfield++ studies of different gas mixtures were done in connection with the Master's thesis of one of the Howard students.

2.5.2 Proposed TOF R&D Activities

We propose to continue with the anti-static mylar mRPC development over the next year, since we believe this may provide not only the cheapest but also the best performing design for the mRPC. Simulation studies will continue to help guide other parameter changes that will help with the resolution, such as the gas mixture and the gap spacing. We also will test and study the preamps in more detail. Besides just using them in the detector, students will measure the analog bandwidth of each component in our readout chain, from the cables, to the preamp, to the digitizer, so that we can understand where the limitations are. Such detailed understanding will also be necessary to model the electronics response when we go to compare our simulations to the measured signals. After the testing of the preamps, we may build a 2nd revision of the board.

One major effort over the next year will be to develop a DRS4 based prototype digitizer board. This will allow us to increase the channels we can read out, and thus will greatly speed up our detector testing. The board will include mostly only the analog sections, the DRS4 and ADCs. It will be controlled and read out with an existing FEM board that was used for the PHENIX MPC-EX detector. This board is based on an ATMEL FPGA, and has enough I/O to read out the DRS4 prototype board. In fact, a first schematic has been made, which is easier than it sounds since we have relied heavily on the open-source DRS4 evaluation board schematics. After a review, the layout should begin around the end of this summer.

Studies of the timing resolution of the UV-sensitive MCP-PMT made by ANL will be done. We will begin with measurements of the QE from 170-600 nm, the TTS over that QE range, the TTS as a function of different HV (across different sections of the PMT), and the timing resolution vs number of photoelectrons. The latter is to check if the resolutions scale as it should. Studies of the TTS vs wavelength will help elucidate the mechanism for the surprising increase in QE as one goes down to 170 nm.

A test beam is proposed for sometime in 2017 to test the variations of mRPCs we will produce, and the TOF MCP-PMT. One major issue during the test beam run in April at the FTBF was the lack of manpower, so we ask for travel money to support 2 weeks of travel for 6 people to go to the FTBF.

2.5.3 TOF R&D Deliverables

FY17

- Anti-static mylar mRPC will be produced and tested in cosmic rays and test beam
- 3D printed mRPC will be tested in cosmic rays, and more test beam if needed
- DRS4 prototype digitization board will be built and tested
- UV sensitive MCP-PMT will be characterized in detail for its timing capabilities with lasers, and tested with cosmic rays and test beam
- Garfield++ simulation of mRPCs will continue to be developed

FY18

- Further building and testing of mRPC variants will be done, with the goal of trying to achieve 10 ps resolution
- The UV sensitive MCP-PMT will continue to be tested, with a goal of 5 ps

3. Lepton (electron) identification

Contacts: Y. Furletova <yulia@jlab.org>, C. Hyde <hyde@odu.edu>

At an Electron-Ion Collider, detection and identification of the scattered electron is a critical requirement. Many important process also involve particles decays to leptons (e.g., J/ψ to e^+e^-). The baseline system for e/π identification is the electromagnetic calorimeter (EM cal), which is included in all the EIC model detectors with 4π coverage. However, the pion suppression achievable in EM cal is limited, for instance, by charge exchange reactions (π^+p to π^0n), which then results in an electromagnetic shower indistinguishable from an electron and associated with a charged track. Although different types of EM calorimeters are considered for different parts of the EIC detectors, in general a good EM cal will provide e/π suppression up to about 1:100. The Cherenkov detectors developed by the PID consortium for hadron ID also provide a supplementary e/π ID capability, and backgrounds can be further reduced through analysis cuts, but in order to reach kinematics where pion backgrounds are high, additional e/π ID detectors would be needed. In the hadron endcap, all EIC model detectors include hadronic calorimeters (Hcal) which also can be used for this purpose (together with the EM cal and the dual-radiator RICH).

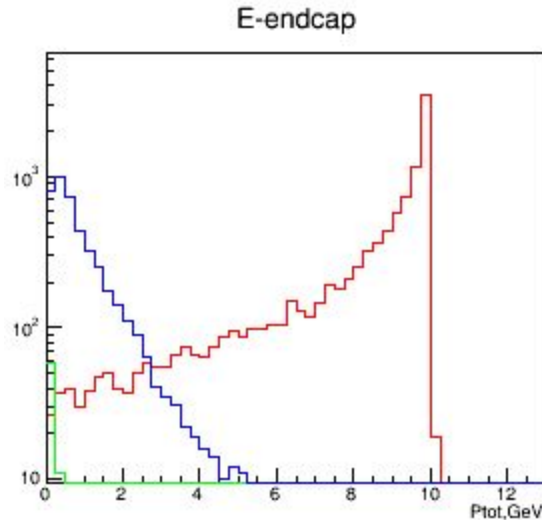


Figure 3.1: Momentum distributions of scattered electrons (red), negative pions (blue), and secondaries (green) hitting the electron endcap for collisions between 10 GeV electrons and 100 GeV protons (a common BNL / JLab kinematic) from Pythia in a bin of $1 < Q^2 < 10 \text{ GeV}^2$ for the electrons (pions include photoproduction). To extend the kinematic coverage to low momenta (high y , low x), better e/π discrimination is required than can be provided by an electromagnetic calorimeter.

However, on the electron side, where Fig. 3.1 shows large the background from low-momentum pions, the use of an Hcal is not required for the physics program of an EIC. As an alternative means of e/π ID,

we thus propose (although we do not request funds for FY17) the development of an e/π Cherenkov detector for the electron endcap - a common solution in electron scattering experiments (including CLAS12, SoLID, *etc.*). The technology we would like to pursue for the R&D is a variation of the Hadron Blind Detector (HBD) used at PHENIX, but with the sensors at the endcaps of the cylinder rather than around the barrel. Since there are here obvious synergies with the activities of eRD6, it would be natural to pursue this project jointly. In the future, it could also be interesting to investigate the option of adding tracking capabilities to this version of the HBD (also turning it into a radial TPC), as well as to investigate the possibilities of enhancing the PID integration with other tracking systems.

4. Photosensors & Electronics

Although readout solutions for DIRC and RICH detectors are not an original problem, the specific requirements these detectors must fulfill within the scope of the EIC pose unique constraints on sensor and electronics performance different from any previous DIRC and/or RICH implementation. Table 1 below lists the minimum requirements on DIRC, modular RICH and Dual-radiator RICH photosensors. Specifically, the small pixel size of 2–3 mm and the immunity to magnetic fields of up to 3 T are unique constraints. The main objective of this R&D effort during the proposed funding period is to identify and assess suitable photosensor and electronics solutions for the readout of the EIC Cherenkov detectors, both for the full EIC detector and for prototypes in beam tests. Depending on the evaluation outcome, design optimization studies of those photosensor and electronics parameters, found lacking in the evaluated samples but critical for operations in the EIC environment, will be carried out. In addition to supporting the adaptation of developing photosensor technologies for the EIC Cherenkov detectors (such as LAPPDs and GEMs) the goal is to identify a cost-efficient common readout solution that is shared within the EIC-PID consortium. Ultimately, in the long term, this R&D work will allow us to make a recommendation about the best photosensors and electronics solutions for the PID detectors in EIC implementation.

Sensor requirements and options

The consideration of possible photosensor solutions for each detector component is driven by the operational parameters of the detector, with cost optimization in mind. The table below summarizes the performance parameters, which photosensors for DIRC, mRICH, and Dual-Radiator RICH must satisfy.

Parameter	DIRC	mRICH	Dual-Radiator RICH
Gain	$\sim 10^6$	$\sim 10^6$	$\sim 10^6$
Timing Resolution	≤ 100 ps	≤ 800 ps	≤ 800 ps
Pixel Size	2-3 mm	≤ 3 mm	≤ 3 mm
Dark Noise	$\leq 1\text{kHz/cm}^2$	$\leq 5\text{MHz/cm}^2$	$\leq 5\text{MHz/cm}^2$

Radiation Hardness	Yes ¹	Yes ¹	Yes ¹
Single-photon mode operation?	Yes	Yes	Yes
Magnetic-field immunity?	Yes (1.5–3 T)	Yes (1.5–3 T)	Yes (1.5–3 T)
Photon Detection Efficiency	$\geq 20\%$	$\geq 20\%$	$\geq 20\%$

Table 1 A list of performance requirements for the photosensors for the EIC PID Cherenkov detectors.

Photomultipliers (PMTs) from the currently available pool that are viable candidates for EIC application are Silicon PMTs (SiPMs), Multi-anode PMTs (MaPMTs), commercial Microchannel-Plate PMTs (MCP-PMTs), Large-Area Picosecond Photodetectors (LAPPDs), and Gaseous Electron Multipliers (GEMs).

The key parameters of the photodetectors for the mRICH are small pixel size, resistance to magnetic field, and low cost (due to its large sensor area). Depending on the mRICH location, the requirement for radiation hardness will vary. The detector does not require good PMT timing resolution. GEMs with a photocathode sensitive to visible light, with their good radiation hardness and good position resolution, would be a very good and cost effective solution for the mRICH. SiPMs could be used if their radiation hardness is sufficient. LAPPDs with pixelized readout could be considered as possible photosensors for mRICH detectors if they have resistance to magnetic fields and low cost. MCP-PMTs satisfy the mRICH requirements, however their high cost is a drawback. The key parameter of the photodetectors for the Dual-radiator RICH is the small pixel size. Although the relative sensor area (normalized to the absolute detector area) of this detector is small, due to the large absolute detector area, cost is also an important parameter. Good sensor options for the Dual RICH would be similar to the ones for mRICH (keeping in mind that due to the location of the sensors, the requirement for radiation hardness is not as important for the Dual RICH). The key parameters of the photodetectors for a DIRC are fast timing, small pixel size, and a moderate to low dark count rate (DCR). Magnetic-field tolerance is required if the DIRC readout is located within the magnetic field of the solenoid. SiPMs could eventually be possible for DIRC if future developments lower their DCR to an acceptable level. Currently, the only photodetectors satisfying these requirements are MCP-PMTs (including LAPPDs with pixelized readout). Excellent timing resolution (~ 100 ps) is in particular required for the high-performance DIRC if a time-based PID reconstruction method is adopted for the geometry based on wide radiator plates. Such timing resolution is satisfied by currently commercially available MCP-PMTs, however, development of electronics with good time resolution for small signals may be required.

4.1 Sensors in High-B fields

Contacts: Y. Ilieva <jordanka@physics.sc.edu>, C. Zorn <zorn@jlab.org>

¹ The EIC radiation levels are expected to be comparable to the levels at current operations of RHIC. The exact level will vary depending on the exact readout location of each PID detector's readout.

The integration of the three Cherenkov detectors in the central detector involves setting their photo-sensor readouts in the non-uniform fringe field of the solenoid. While an out-of-field readout option for the DIRC may be feasible, an in-field readout is the only option for the two RICH detectors. The objective of this activity, thus, has been to assess the gain and the timing performance of available photosensors in high magnetic fields (0T–5T) and for various relative orientations between the sensor and the magnetic field and to reasonably support (as needed for the R&D) further design optimization studies of these sensors. The long-term goal of the research is to recommend sensor options for Cherenkov-detectors readout in the magnetic field of the solenoid magnet.

4.1.1 FY16 Progress and Achievements

The program for testing photosensors in high magnetic fields was established within eRD4, and has now been taking data for a third year. During the last three years we evaluated the gain of commercially available MCP-PMTs in magnetic fields up to 5 T. In 2014 the gain of 3- μm and 6- μm pore-size single-anode sensors was mapped as a function of B-field magnitude and of different orientations of the sensor relative to the magnetic field. The measurements yielded that overall the sensors had a reasonable performance up to 2 T, although that upper limit depended on the sensor, the applied high voltage, and the orientation of the sensor relative to the field. For example, at $\theta=0^\circ$ the 3- μm sensor could be operated up to 5 T. Large gain variations (of about an order of magnitude), depending on the sensor type, with $(B, \theta, \varphi)^2$ were also observed. For example, at $\theta>0^\circ$ the 3- μm sensor could be operated only up to 2 T. Since the readout of the EIC Cherenkov detectors is considered to be in an area where the solenoid field is non-uniform, finding a way to recover the gain not only at large B , but also for a large range of relative orientations between the sensor and the B-field is critical. The simplest means to pursue gain-recovery studies is to vary the voltage distribution within the PMT, as the voltage is an easily accessible operational parameter.

In Summer 2015 we performed further gain studies varying independently the voltages across the three stages: between the photocathode and the MCP (V_{C-MCP}), across the two microchannel plates ($V_{MCP-MCP}$), and between the last MCP and the anode (V_{MCP-A}). The studies were carried out successfully and showed that optimizing the voltage across the multi-channel plates can help to recover the gain in B-fields. However, the range of B-field magnitude over which the gain can be fully recovered strongly depends on the angle between the sensor and the field axes. For $\theta=0^\circ$, a gain of 3.5×10^5 can be recovered up to field magnitudes of 5 T. At $\theta = 10^\circ$, the gain can be recovered for fields below 3 T. At $\theta = 20^\circ$, the gain can be recovered for fields below 2 T. At $\theta = 40^\circ$, the gain can be recovered for fields below 1 T. This means that high-voltage optimization alone cannot achieve gain recovery and uniformity over a large range of sensor-field orientations in a field of 3 T.

4.1.2 Proposed High-B R&D Activities

To achieve full gain recovery at θ angles different than 0° , other sensor parameters (such as bias angle, ratio of pore-size diameter to channel length, distances between the photocathode and first MCP, between the two MCPs, and the anode and the last MCP) need to be also optimized. Given the prohibitive cost of manufacturing single sensors, each with various geometrical parameters, the most efficient way to

² Here θ is the angle between the sensor and the B-field axes and φ is the rotation angle about the sensor axis.

proceed with further optimization studies is to input the MCP-PMT geometry in a simulation, such as GEANT4, and then proceed to simulate the electron avalanche evolution in various magnetic fields. The total anode charge can then be studied for various sensor parameters. Such studies can establish an optimal set of MCP-PMT operational and design parameters, and their limits, for operating the sensors in a range of field magnitudes and orientations similar to what is expected for DIRC and RICH applications in an EIC detector.

Given the large gain variations with (B, θ, ϕ) observed in our measurements during FY14–15, and the solenoid field non-uniformity in the area where the installation of the DIRC³ readout is considered, it is clear that the gain across the readout will not be uniform. Since the timing resolution of an MCP-PMT depends strongly on the amplitude of the output signal, *i.e.* the sensor's gain, the evolution of the sensors timing response with (B, θ, ϕ, HV) needs to be considered. A theoretical model of the electron avalanche development in the MCP suggests that the transit time spread (TTS) of a straight-channel MCP should not depend on the component of the field parallel to the channel axis⁴. No theoretical input exists regarding the effect of transverse fields. Actual timing measurements of chevron-stacked MCPs exist only for magnetic fields up to 2 T. The study done for the development of the BELLE II TOP counter evaluated the timing resolution of a multi-anode Hamamatsu sensor up to 1.5 T for a fixed orientation of the sensor axis relative to the field and found no significant changes⁵. A more comprehensive study was done for the development of the PANDA DIRC as the timing performance was evaluated not only for varying fields but also for varying orientations between the sensor and the field axes⁶. Within the uncertainties of their measurements, the latter study found only a small deterioration of the time resolution towards higher fields. As this study covered a range of fields up to 2 T only, there are no data mapping MCP-PMT timing response above 2 T and it is not known if the observed small deterioration would follow a progressive trend at higher fields. While, based on the published low-field measurements, one expects the timing resolution to deteriorate (if indeed) as the field increases much less than the gain, given the requirement of 100 ps or better timing resolution for the EIC DIRC, it becomes important to evaluate MCP-PMT timing characteristics with (B, θ, ϕ, HV) . Naturally, timing measurements will strongly relate to the gain measurements and will also follow up with sensor design optimization as well as with advancements in performance of timing readout electronics. Extending the functionality of the High-B sensor test facility to allow for precise timing measurements is also a natural synergistic activity with the LAPPD project.

Our goal for the future effort of the High-B program is to achieve an MCP-PMT design and operational parameters that are optimized for successful application in the Cherenkov PID detectors in the high magnetic field of the central detector at EIC. This effort will involve (a) High-B gain measurements of a variety of commercially available multi-anode MCP-PMTs as a function of various operational parameters (b) Development and implementation of a GEANT4 simulation of an MCP-PMT in the design process, (c) Timing studies in high magnetic fields of various commercially available MCP-PMTs.

The proposed activities for FY17 and FY18 are outlined below.

³ DIRC is explicitly mentioned here, since excellent timing resolution is key for the DIRC time-based PID method..

⁴ G.W. Fraser, Nucl. Instr. Meth. **A 291**, 595 (1990).

⁵ S. Hirose, Nucl. Instr. Meth. **A 766**, 163 (2014).

⁶ A. Lehmann *et al.*, Nucl. Instr. Meth. **A 595**, 173 (2008).

FY17

- Measurements of the gain of Photonis (25- μm pore size) and Hamamatsu (10- μm pore size) multi-anode MCP PMTs as a function of $(B, \theta, \phi, \text{HV})$. The Hamamatsu sensor is particularly very interesting since it has a high potential difference also across the gap between the two MCPs (the Photonis sensors have 0-V across the gap). To accomplish full gain scans, we plan to have two runs with cold magnet. Due to the decrease of manpower for these activities at JLab in the second half of 2016 (due to colleagues moving to new employments), to support the preparation and the runs at JLab, funding for one additional undergraduate USC student is requested for both FY17 and FY18.
- Setup modifications for timing studies. The timing resolution of the trigger signal of the pulser driving the LED in our current setup is of the order of few nanoseconds, which is by far inadequate to map a PMT timing resolution at the scale of ≤ 50 ps. Thus, the critical component for timing-resolution measurements in our setup is a high-resolution light source, such as a fast laser. To study TTS in high magnetic fields, a laser with resolution of about 20 ps would be the best. Due to the high cost of such a light source, we plan to use the existing Hall-D laser at JLab. Its resolution is about 50 ps, which rules out TTS studies, but will allow to assess if the overall resolution of the MCP deteriorates to the extent that the limiting value of the overall DIRC resolution of 100 ps would be exceeded. In order to be able to use the Hall-D laser, a custom dark box housing the laser and associated optics (focusing lenses and intensity attenuation filters) needs to be designed and manufactured. The laser light will then be exported to the sensor via optical fiber. The dark box holding the measured sensors needs to be also equipped with a safety interlock, which turns the laser off if the box is accidentally opened during measurements. Such a box could be adapted to hold a different laser should the need arise to acquire a faster laser. The laser box will be also used for the LAPPD activities of this R&D.
- Start of development of MCP-PMT simulation.

FY18

- Measurements of gain and timing resolution of multi-anode MCP PMTs as a function of $(B, \theta, \phi, \text{HV})$.
- MCP-PMT simulation studies.

The proposed activities of the program are based on our results from the first three program years. As our effort grows, we will continue to benefit from the expertise of our PANDA GSI collaborators and from the established collaborations with MCP-PMT manufacturers, such as Photek, Photonis, and Hamamatsu as we proceed with the evaluation of their sensors.

4.1.3 High-B R&D Deliverables

FY17

- Submission of our FY14–15 results for publication.
- Design and manufacturing of laser-adapted optical box.
- Report of multi-anode PMT (Planacon, Hamamatsu) gain as a function of $(B, \theta, \phi, \text{HV})$.

FY18

- Report on multi-anode PMT (Planacon, Hamamatsu) timing resolution as a function of $(B, \theta, \phi, \text{HV})$.

- Progress report on MCP-PMT simulation studies.

4.2 LAPPD™ MCP-PMTs

Contacts: J. Xie <jxie@anl.gov>, M. Chiu <chiu@bnl.gov>

The LAPPD™ project is a multi-year project involving a number of institution, with a goal to create an MCP-PMT that has the same very high performance as existing MCP-PMTs, but at a significantly lower cost. In February of 2016, a DOE review of Detector R&D was held at Argonne that included a review of the LAPPD™ project. Results presented at the review showed that LAPPD™ MCP-PMTs have high photon detection efficiency (15-25%), high gain (10^7), and excellent timing resolution (< 50 ps TTS/photoelectron). As part of the project, Incom, Inc., was awarded a DOE SBIR Phase II contract in April of 2014 to develop a pilot line to demonstrate commercial production of 20×20 cm² LAPPD devices. This SBIR covers the full range of equipment and techniques to produce the device from start to finish, and their goal is a cost that is at least an order of magnitude cheaper than existing MCP-PMTs. If Incom is successful, this would significantly reduce the cost of any MCP-PMT based detector at the EIC, possibly benefiting all the proposed detectors in this proposal (DIRC, RICH, and TOF). Incom is currently close to being able to produce a fully functional device; the remaining hurdle is consistently making ultra-high vacuum seals of the tubes. It should be possible to receive devices in FY17 from Incom for testing.

While the commercial LAPPD MCP-PMT's are promising, the design needs to be optimized for EIC PID applications. Argonne National Laboratories (ANL), which is a charter member of the LAPPD project, has a tile facility to make 6×6 cm² R&D versions of the MCP-PMTs and has served as the basis for the R&D proposed by eRD14 to improve the designs. The facility at Argonne has been successful at making a second generation of samples that have produced both high gain ($> 10^7$) and excellent timing resolution ($\sigma_{\text{TTS}} \sim 20$ ps), with good uniformity in both gain ($< 10\%$) and quantum efficiency (13%), that also demonstrates a reliable sealing technology based on a hermetic thermo-compression indium seal. Over the past year, ANL has provided eRD14 MCP-PMTs for tests of their magnetic field susceptibility, and also a MCP-PMT with a UV fused silica window to check for QE sensitivity down to ~ 170 nm.

In the magnetic field susceptibility tests, we have found that these MCP-PMTs have a very poor response to B-fields compared to MCP-PMTs from other vendors. This is probably due to the large 2 mm gap between the two MCPs in the device. The gap in other MCP-PMTs, such as those from Photonis, is much smaller. The large gap between the MCPs in the LAPPD design allows more deflection of the electrons as they transit the gap, thus lowering the gain.

The UV sensitive MCP-PMT has the potential to increase the photoelectron count by up to a factor of 2 for Cerenkov applications, thus benefiting the TOF, DIRC, and RICH proposals that utilize MCP-PMTs. This takes advantage of the steep rise of the Cherenkov spectrum at lower wavelengths. The increase in photoelectron yield relies also on having good quantum efficiency in the LAPPD photocathode, K₂CsSb, from 300 nm down to 170 nm, which are the borosilicate glass and the fused silica limits, respectively.

One final requirement of many of the EIC PID detectors is for a pixelated readout. This is demanded by imaging detectors such as the DIRC or the RICH detectors, and the LAPPD design currently has strip-line readout. We proposed a couple of possible approaches to provide a pixelated readout. One way would be to replace the stripline with a resistive anode, such as graphite, and put copper pads for capacitive pickup on the other side of the glass base. A scheme like this is used successfully in the mRPC readout. The second way would be to simply have a base with feed-through pins to bring the signals out from pads that are inside the tube. In a related effort, Innosys, Inc. will develop a pad-based readout scheme for the full size LAPPD devices that will allow for a multichannel readout scheme akin to the methods available in current multichannel devices by Photonis and Hamamatsu.

4.2.1 FY16 Progress and Achievements

FY16 was a momentous year for the ANL tile facility, with the ANL group producing several MCP-PMTs for testing by eRD14. As mentioned above, and reported in the January 2016 eRD14 progress report, studies of the magnetic field dependence showed that the LAPPD MCP-PMTs performed very poorly in even relatively weak fields. This shows how feedback from the testing by eRD14 is essential to producing a final design that will satisfy the requirements for EIC PID.

A rate capability study was also done using the 120 GeV proton beam at the FTBF. The protons produce a signal through the Cherenkov light in the 3mm window, as well as from direct emission of electrons in the MCPs. The beam spot size at the FTBF is about 8 mm², and the intensity was varied to achieve fluxes from 3.3-150 kHz/cm²/s. The spectra from these runs are plotted on the left of Fig. 4.2.1, where one can see that the spectra are not modified until after the run with a flux of 75 kHz/cm²/s. This rate capability is above what is required at the EIC, except perhaps at the most forward rapidities. Note that this was for a tube running at a gain of 10⁷, so that even higher rate capabilities could be achieved with lower gain.

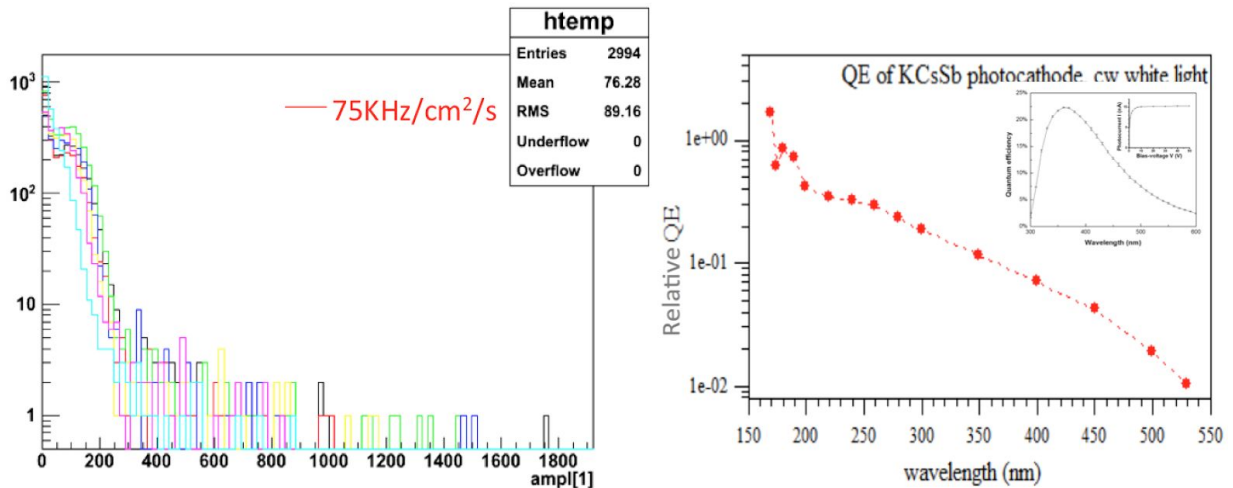


Figure 4.2.1 (Left) Spectra for 120 GeV protons at different intensities incident on a MCP-PMT. Only at fluxes above 75 kHz/cm²/s is the spectral shape affected. (Right) Relative QE of the LAPPD photocathode down to 170 nm. The inset shows the cutoff at 300 nm from the standard LAPPD glass window.

A preliminary relative QE measurement was done at BNL, and shows that wavelengths, below the wavelength cutoff from the borosilicate glass that is used by the LAPPD collaboration. This shows that it might be possible to double the photoelectron yield simply by replacing the window. In April ANL produced a version of the MCP-PMT with a UV-grade fused silica window that will be studied in more detail in FY17.

4.2.2 Proposed LAPPD R&D Activities

FY17

- Studies of the QE of the UV-sensitive MCP-PMT produced by ANL will be completed at BNL. A measurement of the QE, as well as the TTS, will be done vs. wavelength down to 170 nm.
- ANL will produce a modified MCP-PMT with a much smaller gap between the two MCPs. This will then be tested to see if this enhances their capabilities in a magnetic field.
- ANL will produce a version of the MCP-PMT with a pixelated readout. This can be achieved either using a ceramic base with feed-through pins, or via capacitive pickup through a resistive anode.
- If possible, we will procure a 20x20 cm² MCP-PMT from Incom, and initial basic studies of the time resolution, position resolution, and magnetic field susceptibility will be done. Due to the large size of these MCP-PMTs, the high B-field tests will need to be done at ANL in the g-2 magnet test facility.

FY18

- Finalize testing of the pixelated readout in test beam at Fermilab.
- Finish testing of the Incom MCP-PMT in test beam at Fermilab.

4.2.3 LAPPD R&D Deliverables

FY17

- MCP-PMT with better capabilities in a magnetic field, and tests in a field
- MCP-PMT with 3mm pixelated readout
- Tests of UV sensitive MCP-PMT

FY18

- Finalize testing of MCP-PMTs

4.3 GEM photocathodes

Contacts: D. Fields <fields@unm.edu>, H. van Hecke <hubert@lanl.gov>

For FY16 we proposed the development of GEM photocathodes that would provide an ideal low-cost sensor solution for the mRICH and other Cherenkov detectors. We are not requesting funding for the GEMs in FY17, but we are considering to make such a request for FY18.

4.4 Readout Sensors and Electronics for Detector Prototypes

Contacts: F. Barbosa <barbosa@jlab.org>, M. Contalbrigo <mcontalb@fe.infn.it>

As the R&D activities develop towards construction of detector prototypes and carrying out beam tests of these prototypes in order to demonstrate their PID capabilities, the demand arises to instrument the prototypes with small-pixel-size PMTs and the corresponding readout electronics. The DIRC and mRICH prototypes do exist and proof-of-principle beam tests (with borrowed large pixel-size PMTs and corresponding electronics) were successfully carried out with both in FY16. Another beam test with PID capability is foreseen in FY17 for the modular RICH, while a prototype construction for the dual-radiator RICH is planned in FY18. To demonstrate the PID capabilities as required for EIC implementation, all of the prototypes need readout PMTs with 3-mm pixel size. Potential sensor solutions could be MaPMTs, SiPMs, or/and MCP-PMTs. A common readout solution, which can be shared between the three detector prototypes, would be ideal. To identify the most cost-efficient option(s), however, all possible PMT solutions need to be assessed. This evaluation has already begun within the consortium and will be concluded during FY17.

While, we have been assessing various small-pixel size sensor options, it has become evident that a dedicated parallel effort in developing the electronics to read out the sensors is necessary. Efforts to borrow already existing electronics readout from Hall-D at JLab (which uses 3-mm pixel-size SiPMs for their calorimeter) were unsuccessful as all procured readout chips are in use. Purchasing the exact same chip from Hamamatsu (custom made for Hall D) is not a viable option. Another option would be to use the electronics designed for Hall-B RICH⁷. However, since the Hall-B RICH is equipped with 6-mm pixel-size PMTs, that design cannot be directly copied but an adaptation needs to be developed. After extensive discussions within the consortium and with electronics expert groups (JLab and INFN), it has been recognized that the instrumentation of the prototypes with readout requires dedicated electronics development, independent of what the PMT solution(s) for the prototypes would be. It is also apparent that the development will have to be staged.

To optimize cost and to benefit maximally from synergies with expert groups who have expressed interest to collaborate, such as JLab (F. Barbossa), INFN (M. Contalbrigo), Northwestern Polytechnical University, China (Prof. Wei), and University of Hawaii (G. Varner), in FY17 we will carry out a detailed investigation of the most optimal way to develop the electronics readout. In parallel to this activity, we plan to procure in FY17 one unit of H13700 MaPMT with 3-mm pixel size (256 channels) and to borrow several units of 3-mm pixel-size SiPMs from the JLab detector group. To readout these sensors, the electronics solution for the Hall-B RICH will be modified. This activity will make extensive use of existing components, equipment, and infrastructure developed for the High-B RICH and will make use of the expertise of the INFN and the JLab electronics groups. The purpose of acquiring and reading out a limited set of 3-mm pixel-size sensors is twofold: on one hand, the set will be sufficient to instrument the mRICH prototype for a beam test in Summer 2017; on another hand, the adaptation of the existing

⁷ M. Contalbrigo, Nucl. Instrum. Methods A 787, 224 (2015).

electronics and the beam test will provide initial experience with reading out small-pixel-size PMTs. The beam test of the mRICH prototype is a critical activity for demonstrating the PID capability of the device and for the assessment of the photon-detector and readout performance required in realistic conditions. The experience with reading out 3-mm pixel-size PMTs will provide a valuable input to the assessment and planning of electronics readout options of all the Cherenkov prototypes.

Thus, by the end of FY17, we will be able to formulate a staged plan (proposed activities and budgets for FY18 and the following years) for development of the electronics readout of the RICH and DIRC prototypes.

This timeline is consistent with the timeline of identifying the best PMT solution and also with the timelines of the future DIRC and mRICH prototype beam tests and the construction of the dual-radiator RICH prototype. Ultimately, in the long term, the R&D activities proposed here to instrument the Cherenkov prototypes will support the development of the final readout solution for the EIC PID detectors.

4.4.1 Proposed R&D Activities

FY17

- Investigation of the most optimal PMT solution(s) for the RICH and DIRC prototypes.
- Investigation of the most optimal and cost efficient way to develop the electronics readout(s) for the RICH and DIRC prototypes.
- Modification of the Hall-B RICH electronics solution to readout 3mm-pixel-size PMTs: H13700 and SiPMs, and to instrument mRICH prototype for FY17 beam test.
- Workshop on electronics solutions for RICH and DIRC prototypes.

FY18

- Acquisition of PMTs.
- Development of electronics readout.

4.4.2 Proposed R&D Deliverables

FY17

- Staged plan outlining the path to instrument the prototypes with readouts.

FY18

- Design report on electronics solution with a prototype.

5. Budget

5.1 Budget Request

We request \$443k for FY17, and estimate an additional \$515k for FY18. All budgets include overhead by the receiving institution. A breakdown of the request by year, project, and institution can be found below. Compared with FY16, we have reduced the number of institutions which receive funding to increase the

flexibility in using consortium funds, in particular for travel. The FY17 SOWs will be submitted with a wording reflecting the possibility for some institutions to fund collaborators at other institutions.

5.2 Dual-Radiator RICH

FY17

1. Postdoc (100%, Alessio Del Dotto, INFN/JLab): \$55k

Total: \$55k

FY18

1. Postdoc (100%, Alessio Del Dotto, INFN/JLab): \$55k
2. Prototype (Duke): \$20k (aerogel tile (n=1.02), materials & gas)

Total: \$75k

5.3 Modular RICH

FY17

Postdoc (50% salary, Sawaiz Syed at GSU): \$45k

Graduate student (Cheuk-Ping Wong at GSU): \$30k

Travel (beam test): \$10k (GSU)

Total: \$85k

FY18

Postdoc (50% salary, Sawaiz Syed at GSU): \$45k

Graduate student (Cheuk-Ping Wong at GSU): \$30k

Travel: \$10k (GSU)

Total: \$85k

5.4 DIRC

FY17

Procurement: Radiation hard, three-layer lens (for high-performance DIRC): \$11k (CUA)

Postdoc ($\frac{3}{4}$ of year 50%): \$33k (CUA)

Undergraduate Student: \$8k (CUA)

Graduate Student: \$20k (ODU)

Travel: \$25k (ODU 5k; CUA 20k for all other travel, including GSI)

Total: \$98k

FY18

Costs associated with transport of PANDA prototype from GSI to CUA: \$10k

Postdoc (50%): \$44k (CUA)

Undergraduate Student: \$8k (CUA)

Travel: \$25k (ODU 5k; CUA 20k for all other travel, including GSI)

Total: \$87k

5.5 TOF

FY17

1. Materials for Prototype Electronics + mRPC Development (BNL): \$25K
2. Travel (BNL): \$15K

Total: \$40k

FY18

1. Materials Electronics + mRPC Development (BNL): \$25K
2. Travel (BNL): \$15K

Total: \$40k

5.6 Sensors in High-B Fields

FY17

1. Timing upgrade for high-B test facility (JLab):
 - a. Laser Box, optics, and safety: \$10k
2. Liquid Helium, high-B test facility (JLab): \$12k
3. Shipping cost of MCP-PMTs on loan (JLab): \$2k
4. High-B components (sensor holders, dark box cap modifications, *etc.*) (JLab): \$3k
5. Undergraduate students (USC): \$15k
6. Travel (USC): \$13k

Total: \$55k

FY18

1. Timing upgrade for high-B test facility:
 - a. High-resolution TDC and Fast Constant Fraction Discriminator: \$15k (JLab)
2. Liquid Helium: \$12k (JLab)
3. High-B components (sensor holders, dark box cap modifications, *etc.*): \$3k (JLab)
4. Shipping cost of MCP-PMTs on loan: \$2k (JLab)
5. Undergraduate students (USC): \$15k
6. Travel (USC): \$13k

Total: \$60k

5.7 LAPPDs

FY17

1. 0.2 FTE Post-doc (ANL): \$25k
2. 0.1 FTE Scientist (ANL): \$25k
3. 0.1 FTE Technician (ANL): \$25k
4. Materials (ANL): \$5k
5. Travel (ANL): \$10k

Total: \$90k

FY18

1. 0.2 FTE Post-doc (ANL): \$25k
2. 0.1 FTE Scientist (ANL): \$25k
3. Travel: \$6k

Total: \$56k

5.8 Readout Sensors and Electronics for Detector Prototypes

FY17

1. Procurement: one MaPMT H13700 (GSU): \$6k
2. Adaptation of existing electronics to readout 3-mm pixel-size sensors - H13700 and SiPMs (JLab): \$15k

Total: \$21k

FY18

Develop a prototype electronics readout for specific sensor solution (JLab):

1. Parts & Materials (ASICs, FPGAs, components, etc): \$17k
2. PCB Services (Fab & Assembly): \$10k
3. Test Fixtures: \$5k
4. Equipment (power supplies, etc): \$20k

Sensors:

1. Specific sensors will depend on identified solution in FY17 (CUA): \$60k

Total: \$112K

5.9 Budget by institution

Budget request by institution (\$329k was awarded for FY16)

	FY17	FY18	<i>Total</i>
ANL	\$90k	\$56k	<i>\$146k</i>
BNL	\$40k	\$40k	<i>\$80k</i>
CUA (and GSI)	\$72k	\$142k	<i>\$214k</i>
Duke	0	\$20k	<i>\$20k</i>
GSU	\$91k	\$85k	<i>\$176k</i>
INFN (JLab)	\$55k	\$55k	<i>\$110k</i>
JLab	\$42k	\$84k	<i>\$126k</i>
ODU	\$25k	\$5k	<i>\$30k</i>
USC	\$28k	\$28k	<i>\$56k</i>
<i>Total</i>	<i>\$443k</i>	<i>\$515k</i>	<i>\$958k</i>

Appendices

Appendix A

List of R&D Publications and Presentations

1. C. Nickle, *Experimental Setup for Magnetic-Field Tests of Small-Size Light Sensors at Jefferson Lab*, poster presentation at the Conference Experience for Undergraduates at the 2013 Fall Meeting of the APS Division of Nuclear Physics, October 23–26, 2013, Newport News, VA; BAPS.2013.DNP.EA.121.
2. E. Bringley *et al.*, *Experimental Setup and Commissioning of a Test Facility for Gain Evaluation of Microchannel-Plate Photomultipliers in High Magnetic Field at Jefferson Lab*, poster presentation at the Conference Experience for Undergraduates at the 4th Joint Meeting of the APS Division of Nuclear Physics and the Physical Society of Japan, October 7–11, 2014, Waikoloa, Hawaii; BAPS.2014.HAW.GB.140.
3. H. Hamilton, *Time of Flight Detector Development for Future Heavy Ion Experiments*, poster presentation at the Conference Experience for Undergraduates at the 4th Joint Meeting of the APS Division of Nuclear Physics and the Physical Society of Japan, October 7–11, 2014, Waikoloa, Hawaii; BAPS.2014.HAW.GB.149.
4. C. Towell, *Developing a High Precision Cosmic Test Stand for PHENIX Research and Development*, poster presentation at the Conference Experience for Undergraduates at the 4th Joint Meeting of the APS Division of Nuclear Physics and the Physical Society of Japan, October 7–11, 2014, Waikoloa, Hawaii; BAPS.2014.HAW.GB.147.
5. H. Hamilton, *Improved Timing Instruments for Particle Identification*, oral presentation at the Abilene Christian University Undergraduate Research Festival, March 31, 2015, Abilene, TX.
6. C. Towell, *Building Detectors to Study a New Phase of Matter*, oral presentation at the Abilene Christian University Undergraduate Research Festival, March 31, 2015, Abilene, TX.

7. E. Bringley *et al.*, *Experimental Setup and Commissioning of a Test Facility for Gain Evaluation of Microchannel-Plate Photomultipliers in High Magnetic Field at Jefferson Lab*, poster presentation at the University of South Carolina Discovery Day, 24 April 2015, Columbia, SC.
8. C. Barber, *Gain Evaluation of Micro-Channel-Plate Photomultipliers in the Upgraded High-B Test Facility at Jefferson Lab*, poster presentation at the Conference Experience for Undergraduates at the 2015 Fall Meeting of the APS Division of Nuclear Physics, October 28–31, 2015, Santa Fe, NM; BAPS.2015.DNP.EA.37.
9. H. Hamilton, *Testing of multigap Resistive Plate Chambers for Electron Ion Collider Detector Development*, poster presentation at the Conference Experience for Undergraduates at the 2015 Fall Meeting of the APS Division of Nuclear Physics, October 28–31, 2015, Santa Fe, NM; BAPS.2015.DNP.EA.9.
10. C. Towell, *Cosmic Test Stand Development for Electron Ion Collider Detector R&D*, poster presentation at the Conference Experience for Undergraduates at the 2015 Fall Meeting of the APS Division of Nuclear Physics, October 28–31, 2015, Santa Fe, NM; BAPS.2015.DNP.EA.20.
11. H. Hamilton, *Testing of Advanced Particle Detectors for the Next Generation Particle Collider*, oral presentation at the Abilene Christian University Undergraduate Research Festival, 5 April 2016, Abilene, TX.
12. C. Towell, *Development of an Electron Ion Collider Detector Test Stand*, oral presentation at the Abilene Christian University Undergraduate Research Festival, 5 April 2016, Abilene, TX.
13. Y. Ilieva for the EIC DIRC Collaboration, *MCP-PMT Studies at the High-B Test Facility at Jefferson Lab*, invited talk at the International Workshop on Fast Cherenkov Detectors - Photon detection, DIRC design and DAQ, November 11–13, 2015, Giessen, Germany.
14. Y. Ilieva *et al.*, *MCP-PMT Studies at the High-B Test Facility at Jefferson Lab*, JINST **11**, 2016; <http://dx.doi.org/10.1088/1748-0221/11/03/C03061>. Proceedings of the International Workshop on Fast Cherenkov Detectors - Photon detection, DIRC design and DAQ, November 11–13, 2015, Giessen, Germany.
15. A. Del Dotto for the EIC PID consortium, *Design and R&D of RICH detectors for EIC experiments*, accepted for RICH 2016, 9th International Workshop on Ring Imaging Cherenkov Detectors, Slovenia on September 5-9, 2016 (proceedings will be published in NIMA).
16. Z.W. Zhao for the EIC PID consortium, *EIC RICH R&D*, presentation at EIC User Group Meeting, January 2016.
17. G. Kalicy for the EIC DIRC Collaboration, *High-performance DIRC detector for Electron Ion Collider*, invited talk at the International Workshop on Fast Cherenkov Detectors - Photon detection, DIRC design and DAQ, November 11–13, 2015, Giessen, Germany.
18. L. Allison for the EIC DIRC Collaboration, *Studies of prototype 3-component lens in CERN test beam and on a test bench at ODU*, invited talk at the International Workshop on Fast Cherenkov Detectors - Photon detection, DIRC design and DAQ, November 11–13, 2015, Giessen, Germany.
19. L. Allison for the EIC DIRC Collaboration, *Particle ID with DIRC Detectors*, invited talk at ODU Nuclear Group Seminar, March 17, 2016.
20. G. Kalicy for the EIC DIRC Collaboration, *DIRCs*, invited talk at ODU Nuclear Group Seminar, December 4, 2016.

21. G. Kalicy *et al.*, High-performance *DIRC detector for Electron Ion Collider*, submitted to JINST, 2016; Proceedings of the International Workshop on Fast Cherenkov Detectors - Photon detection, DIRC design and DAQ, November 11–13, 2015, Giessen, Germany.
22. G. Kalicy for EIC DIRC Collaboration, *DIRC@EIC*, presentation at EIC User Group Meeting, January 2016.
23. G. Kalicy for EIC DIRC Collaboration, *DIRC detectors*, presentation for seminar in JLab, December 2015.
24. G. Kalicy for EIC DIRC Collaboration, *Photosensors tests at high B facility in JLab*, presentation on meeting with Photonis in Lancaster, PA, October 2015.
25. G. Kalicy for EIC DIRC Collaboration, *Photosensors tests at high B facility in JLab*, presentation on meeting with Hamamatsu at JLab, September 2015.
26. G. Kalicy for EIC DIRC Collaboration, *Developing DIRC Technology*, presentation at ODU Colloquium Norfolk VA, April 2015.
27. C.P. Wong, *Simulation Study of RICH Detector for Particle Identification in Forward Region at Electron-Ion Collider*, oral presentation at APS April Meeting 2015, April 11-14, 2015, Baltimore, MD.
28. J. Xie *et al.*, *Planar microchannel plate photomultiplier with VUV-UV-Vis full range response for fast timing and imaging applications*, accepted for RICH 2016, 9th International Workshop on Ring Imaging Cherenkov Detectors, Slovenia on September 5-9, 2016 (proceedings will be published in NIMA).
29. J. Xie *et al.*, *Development of a low-cost fast-timing microchannel plate photodetector*, Nucl. Instrum. Meth. A 824 (2016) 159-161.
30. J. Wang *et al.*, *Development and testing of cost-effective, 6cm \times 6cm MCP-based photodetectors for fast timing applications*, Nucl. Instrum. Meth. A 804 (2015) 84-93.